Available online at www.sciencedirect.com
ScienceDirect
Lithos 91 (2006) 74–94
LITHOS
www.elsevier.com/locate/lithos

Petrogenesis and tectonic setting of the peralkaline Pine Canyon caldera, Trans-Pecos Texas, USA

John Charles White [a,*], S. Christian Benker [a], Minghua Ren [b], Kevin M. Urbanczyk [c], Donald W. Corrick [d]

[a] *Department of Earth Sciences, Eastern Kentucky University, Richmond, KY 40475, USA*
[b] *Department of Geological Sciences, University of Texas at El Paso, El Paso, TX 79968, USA*
[c] *Department of Earth and Physical Sciences, Sul Ross State University, Alpine, TX 79832, USA*
[d] *National Park Service, Big Bend National Park, TX 79834, USA*

Received 4 July 2005; accepted 13 March 2006
Available online 19 May 2006

Abstract

The Pine Canyon caldera is a small (6–7 km diameter) ash-flow caldera that erupted peralkaline quartz trachyte, rhyolite, and high-silica rhyolite lavas and ash-flow tuffs about 33–32 Ma. The Pine Canyon caldera is located in Big Bend National Park, Texas, USA, in the southern part of the Trans-Pecos Magmatic Province (TPMP). The eruptive products of the Pine Canyon caldera are assigned to the South Rim Formation, which represents the silicic end member of a bimodal suite (with a "Daly Gap" between 57 and 62 wt.% SiO_2); the mafic end member consists primarily of alkali basalt to mugearite lavas of the 34–30 Ma Bee Mountain Basalt. Approximately 60–70% crystallization of plagioclase, clinopyroxene, olivine, magnetite, and apatite from alkali basalt coupled with assimilation of shale wall rock (M_a/M_c=0.3–0.4) produced the quartz trachyte magma. Variation within the quartz trachyte–rhyolite suite was the result of ~70% fractional crystallization of an assemblage dominated by alkali feldspar with subordinate clinopyroxene, fayalite, ilmenite, and apatite. High-silica rhyolite is not cogenetic with the quartz trachyte–rhyolite suite, and can be best explained as the result of ~5% partial melting of a mafic granulite in the deep crust under the fluxing influence of fluorine. Variation within the high-silica rhyolite is most likely due to fractional crystallization of alkali feldspar, quartz, magnetite, biotite, and monazite. Lavas and tuffs of the South Rim Formation form A-type rhyolite suites, and are broadly similar to rock series described in anorogenic settings both in terms of petrology and petrogenesis. The Pine Canyon caldera is interpreted to have developed in a post-orogenic tectonic setting, or an early stage of continental rifting, and represents the earliest evidence for continental extension in the TPMP.

Keywords: Peralkaline; Trachyte; Rhyolite; Petrogenesis; Continental extension

1. Introduction and geologic setting

The South Rim Formation (SRF) consists of peralkaline quartz trachyte, rhyolite, and high-silica rhyolite lavas and tuffs that erupted about 33–32 Ma from the Pine Canyon caldera and several postcaldera vents that form the Chisos Mountains in Big Bend National Park

* Corresponding author. Tel.: +1 859 622 1276; fax: +1 859 622 1451.
E-mail address: John.White@eku.edu (J.C. White).

0024-4937/$ - see front matter © 2006 Elsevier B.V. All rights reserved.
doi:10.1016/j.lithos.2006.03.015

(BBNP), Texas, USA (Fig. 1) (Maxwell et al., 1967; Ogley, 1978; Barker et al., 1986; Urbanczyk and White, 2000; Miggins et al., 2004). The SRF represents the silicic end-member of a bimodal suite in BBNP; the mafic end-member consists of alkali basalt to mugearite lavas of the Chisos Group, which includes the 34–30 Ma Bee Mountain Basalt as well as older (47–34 Ma), similar lavas (Schucker, 1986; Schucker and Nelson, 1988; Henry and Davis, 1996).

BBNP is located in the southern part of the Trans-Pecos Magmatic Province (TPMP), one of several middle Tertiary igneous provinces proximal to late Tertiary to Quaternary basins of the Rio Grande rift (Fig. 2; Barker, 1977, 1987; Dickerson and Muehlberger, 1994; Chapin et al., 2004). The TPMP is divided into an eastern alkalic belt and a western metaluminous belt; most alkalic magmatism occurred in the eastern belt, including peralkaline volcanic centers such as the Pine Canyon caldera, the Buckhorn caldera (Parker, 1986), and the Paisano volcano (Parker, 1983), as well as a chain of nepheline trachyte and phonolite intrusions (Potter, 1996). Metaluminous volcanic rocks occur throughout the TPMP, and are closely related both spatially and temporally to peralkaline volcanic centers in the eastern belt (e.g., the Davis Mountains volcanic field; Henry et al., 1994). Mafic rocks are widespread in the southern TPMP (the Big Bend area), but are very rare elsewhere in the TPMP (Barker, 1987).

Magmatism in the TPMP began about 48 Ma, immediately following the end of the Laramide orogeny in west Texas, and continued until about 16 Ma, during Basin and Range extension (Henry and McDowell, 1986). Although it is generally accepted that the earliest magmatism took place in a compressional (orogenic) stress regime, and that the latest magmatism took place in an extensional (intraplate) stress regime, the timing of the change is controversial. On the basis of paleostress

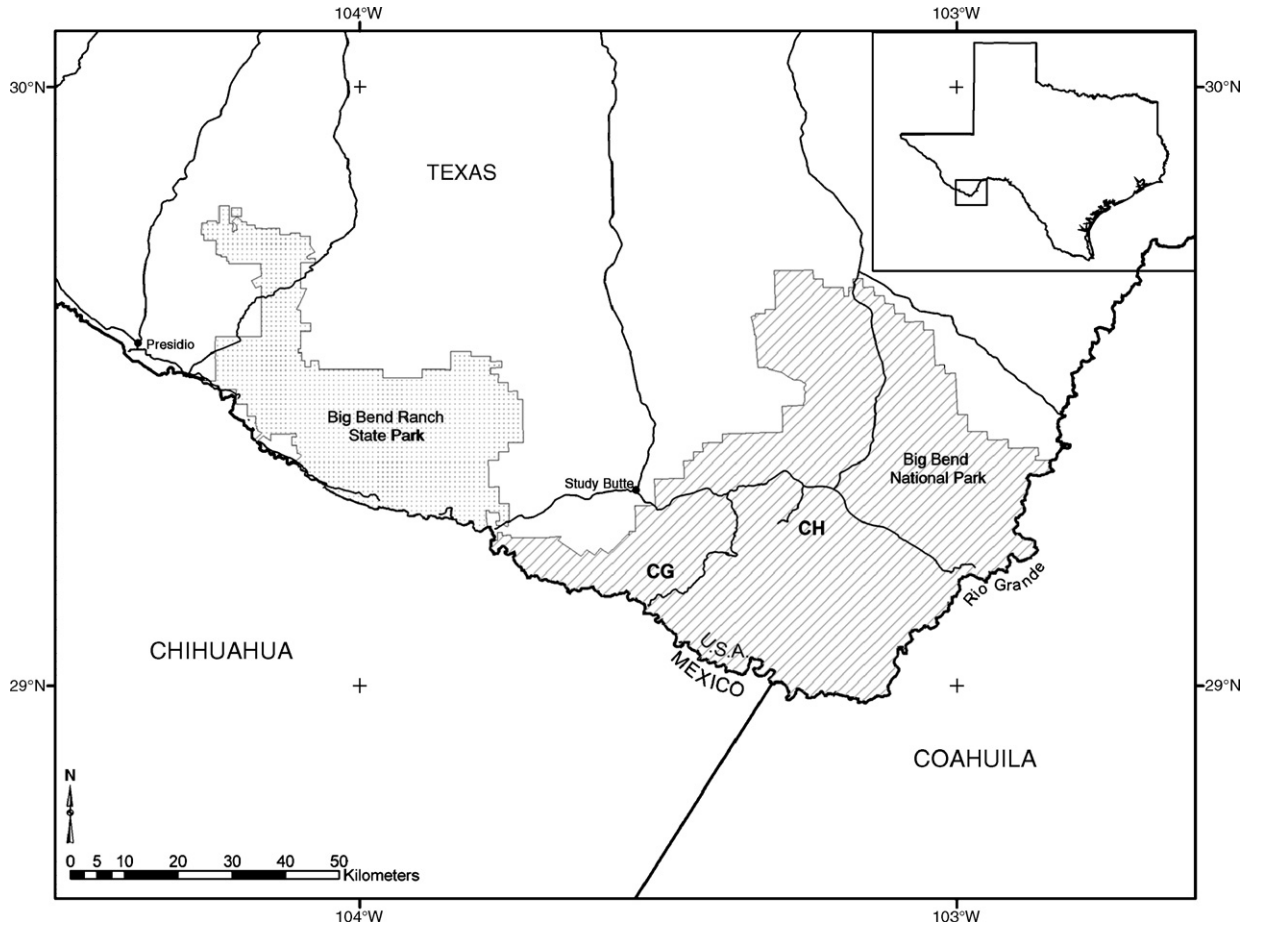

Fig. 1. Location of Big Bend National Park, Texas. Areas within the park referred to in the text include the Chisos Mountains (CH) and the Castolon Graben (CG).

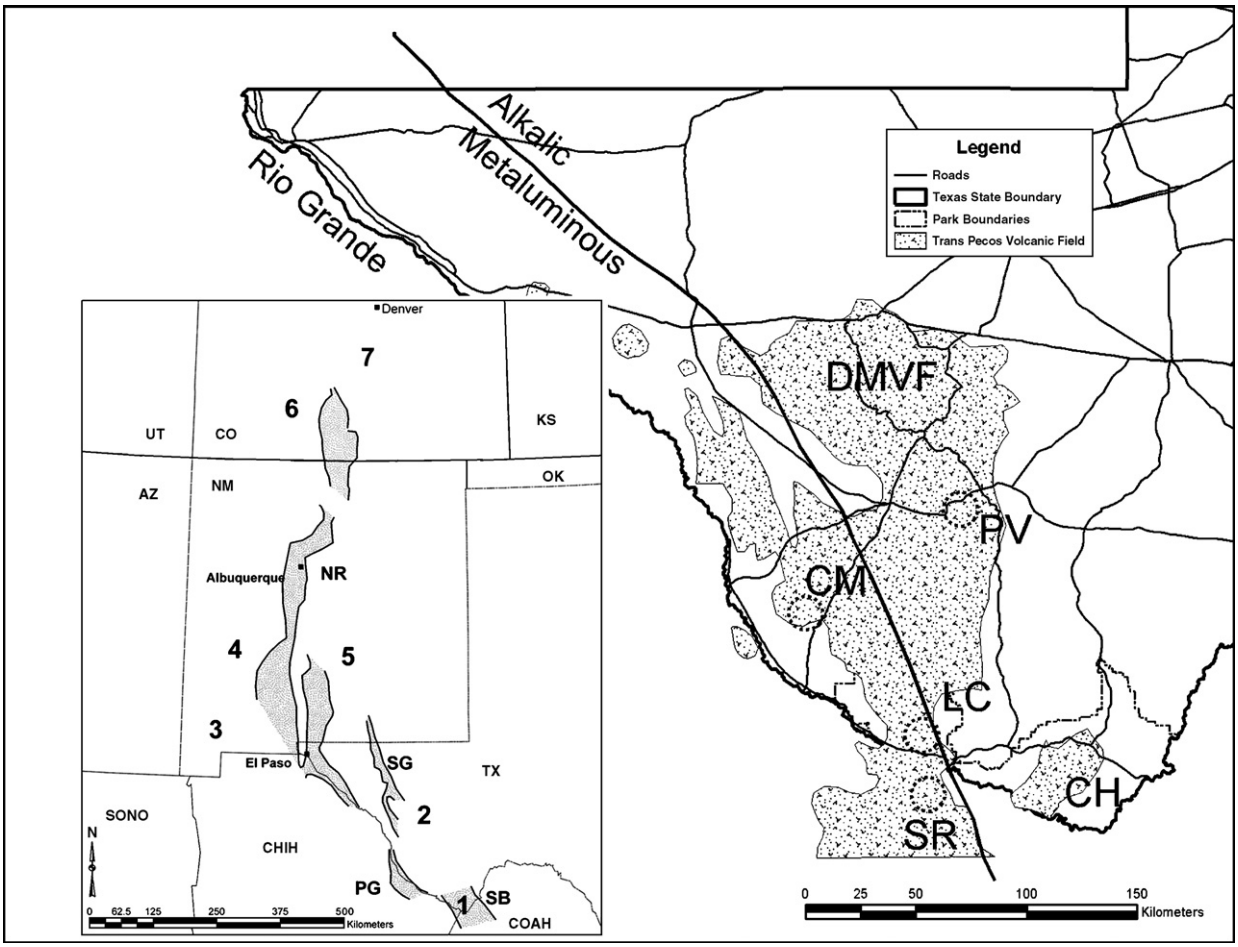

Fig. 2. The Trans-Pecos Magmatic Province (TPMP) with the approximate boundary between the eastern alkalic belt and western metaluminous belt; the shaded area indicates the extent of volcanic rocks in the TPMP (Barker, 1977). Also shown for reference are the national and state part boundaries and roads (see Fig. 1). Volcanic centers include: CH, Chisos Mountains; CM, Chinati Mountains; DMVF, Davis Mountains volcanic field; LC, Leyva Canyon volcano; PV, Paisano volcano; SR, Sierra Rica. The inset map shows the locations of middle to late Tertiary basins of the Rio Grande Rift and selected middle Tertiary volcanic centers. Volcanic centers include: (1) Chisos Mountains, (2) Davis Mountains, (3) Boot Heel, (4) Mogollon–Datil, (5) Sierra Blanca, (6) San Juan Mountains, and (7) central Colorado; basins include: NR, northern Rio Grande rift; SG, Salt Graben; PG, Presidio Graben; and SB, the "Sunken Block" (Dickerson and Muehlberger, 1994; Chapin et al., 2004).

analysis of dikes and veins in the TPMP, Henry et al. (1991) suggested that a compressional regime persisted until 31 Ma, and that magmatism prior to 31 Ma occurred in a subduction-related, continental volcanic arc. However, recent work in southern New Mexico and central Colorado, has suggested that extension began in the region about 36 Ma, and that related magmatism was the result of passive continental rifting over a foundering subducted slab (Lawton and McMillan, 1999; McMillan et al., 2000; Chapin et al., 2004; McIntosh and Chapin, 2004). Alkalic rocks such as peralkaline quartz trachyte and rhyolite are generally considered to be characteristic of intraplate magmatism (Bowden, 1974), but have been documented at convergent margins (e.g., D'Entrecasteaux Islands, New Guinea: Smith et al., 1977; Mayor Island, New Zealand: Houghton et al., 1992). Within volcanic arcs, however, peralkaline magmatism is usually still attributed to extension either during the waning stages of orogeny, or immediately after, in a post-orogenic tectonic regime (Bonin, 1988; Stolz et al., 1993; Bonin et al., 1998; Bonin, 2004; Cadoux et al., 2005).

The petrogenesis of peralkaline rocks and the origin of the "Daly Gap" between mafic and silicic magmas has been the subject of debate for many years, and three leading petrogenetic models have emerged: (1) Protracted fractional crystallization of transitional to alkali basalt (e.g., Baker et al., 1977; Parker, 1983; Mungall and Martin, 1995; Civetta et al., 1998); (2) Low-degree partial melting of alkali-rich mafic rock, followed by

fractional crystallization (Bailey and Macdonald, 1970; Lowenstern and Mahood, 1991; Hay and Wendlandt, 1995; Hay et al., 1995a,b; Bohrson and Reid, 1997, 1998); and, (3) Partial melting of crustal rock or fractional crystallization combined with alkali and trace element enrichment via a volatile phase (Bailey and Macdonald, 1975; Macdonald et al., 1987; Bailey and Macdonald, 1987; Davies and Macdonald, 1987). In this paper, we examine the petrogenesis of a suite of peralkaline quartz trachyte, rhyolite, and high-silica rhyolite that erupted from the Oligocene Pine Canyon caldera. The close spatial and temporal relationship between peralkaline silicic magmas and mafic magmas in the Big Bend area provides an excellent opportunity to evaluate the role of mafic magmatism in the origin of peralkaline magmas. Detailed knowledge of the petrogenesis of the SRF is also applied to help interpret the tectonic setting of the TPMP at 33–32 Ma.

2. Analytical methods

We present sixty new analyses of samples of lava and tuff from the South Rim Formation. All samples were powdered to −200 mesh in a pre-contaminated tungsten-carbide shatterbox grinder. Thirty-seven of these were analyzed for both major- and trace-elements by ICP-OES and ICP-MS techniques following a lithium metaborate/tetraborate fusion dilution at Activation Laboratories, Ancaster, Ontario (Code 4Lithoresearch). The remaining twenty-three were analyzed by electron-dispersive X-ray fluorescence spectroscopy (ED-XRF) at Sul Ross State University, Alpine, Texas; see White and Urbanczyk (2001) for a detailed description of the procedure. Mineral chemistry was obtained by electron probe microanalysis (EPMA) at the University of Texas at El Paso on a Cameca SX50 instrument; a description of the procedure can be found in White et al. (2005). Whole-rock and representative mineral analyses are available on line; see the journal's homepage http://www.elsevier.com/locate/lithos under "Electronic Supplements".

3. Stratigraphy and petrology

3.1. Chisos Group

Maxwell et al. (1967) assigned volcanic units and intercalated sedimentary rocks in the Big Bend area that are located above late Cretaceous and early Tertiary sedimentary rocks, but below a major unconformity marking the end of sedimentary deposition, to the Chisos Formation (promoted to Group by Henry and Davis, 1996). The Chisos Group consists of the 47–34.5 Ma Alamo Creek Basalt (ACB), the 34.5 Ma Ash Spring Basalt (ASB), the 34–30 Ma Bee Mountain Basalt (BMB), the 33 Ma Mule Ears Spring Tuff (MEST), and the 32 Ma Tule Mountain Trachyandesite (TMT) (Henry and McDowell, 1986; Schucker and Nelson, 1988; Henry and Davis, 1996). ASB, BMB, and volcaniclastic sedimentary rocks are the only units in the Chisos Group that crop out in the Pine Canyon area (Maxwell et al., 1967; Ogley, 1978). The BMB is the most widespread volcanic formation in the Chisos Group (Barker et al., 1986), and consists of numerous flows of aphyric to porphyritic alkali basalt to mugearite lavas that erupted over a large area, cropping out from the Chisos Mountains westward into Big Bend Ranch State Park (Schucker, 1986; Henry and Davis, 1996). At least three flows of BMB lava have been identified between the MEST and TMT, and at least one flow has been described above the TMT, indicating activity to at least 32 Ma (Henry and Davis, 1996) and possibly as late as 29 Ma (Schucker and Nelson, 1988).

3.2. South Rim Formation (SRF)

The peralkaline quartz trachyte, rhyolite, and high-silica rhyolite lavas and tuffs that crop out in the Chisos Mountains were assigned by Maxwell et al. (1967) to the South Rim Formation (SRF), along with similar peralkaline high-silica rhyolite lavas and tuffs that crop out to the southwest of the Chisos in the Castolon graben. Benker (2005) divided the SRF in the Chisos Mountains into three informal members that correspond to the three episodes of Pine Canyon volcanism described by Barker et al. (1986): the Pine Canyon Rhyolite Member (PCR), the Boot Rock Member (BRM), and the Emory Peak Rhyolite Member (EPR).

3.2.1. Pine Canyon Rhyolite Member (PCR)

The Pine Canyon Rhyolite ("Brown Rhyolite" of Maxwell et al., 1967) represents the caldera-forming ignimbrite of the Pine Canyon caldera, a small (6–7 km diameter) downsag caldera (Walker, 1984) that formed about 33–32 Ma (Barker et al., 1986). The PCR defines a circular pattern coincident with the caldera itself and ranges in thickness from ~300 m along the northern and eastern margins of the caldera to ~20 m along the southwest margin of the caldera (Ogley, 1978; Drenth and Finn, 2004). PCR ranges in lithology from a lithic-free, densely welded vitrophyre to a coarsely lithic welded ash-flow tuff that weathers to a distinctive brown color. PCR samples studied consist primarily of sparsely phyric, partially

devitrified, eutaxitic vitrophyre. Anorthoclase (Or_{35}) is the dominant phenocryst, comprising about 5 vol.% of the sample. Minor (<1 vol.%) phenocrysts include sodic hedenbergite ($Wo_{46}Fs_{54}$), ilmenite (Ilm_{98}), aenigmatite, ferrorichterite, fayalite, and apatite. The presence of both aenigmatite and ferrorichterite suggest equilibration at low temperatures (<750 °C) and low oxygen fugacities (Charles, 1975; Scaillet and Macdonald, 2001). Oxygen fugacities for sample 99802, calculated from clinopyroxene–quartz–ilmenite equilibria with QUILF95 (Andersen et al., 1993) over a temperature range of 680 to 740 °C at 1 kbar of pressure, are 1.7 to 1.9 log units below the FMQ buffer. These results are consistent with the aenigmatite–ilmenite equilibrium model presented by White et al. (2005), which suggests crystallization between FMQ-1.7 and FMQ-2.0 in a quartz-saturated melt with a $Na_2Si_2O_5$ activity of 1.0.

3.2.2. Boot Rock Member (BRM)

The Boot Rock Member (Wasp Spring Flow-Breccia and Lost Mine Rhyolite of Maxwell et al., 1967) consists of a series of quartz trachyte to rhyolite lavas, ignimbrites, and maar surge deposits that erupted from intra- and extra-caldera postcaldera vents about 32.17±0.9 Ma (Barker et al., 1986; Urbanczyk and White, 2000; Miggins et al., 2004). Inside the caldera structure, the BRM overlies the PCR without a sharp contact, and includes megabreccia, welded ash-flow tuff, surge deposits, and quartz trachyte lava. BRM welded ash-flow tuffs, lavas, and similar intrusive rocks studied consist of <10 vol.% phenocrysts of sanidine (Or_{39}) with subordinate (<1 vol.%) hedenbergite ($Wo_{44}Fs_{55}$) and ilmenite ($Ilm_{96–97}$), and with rare magnetite (Mgt_{37}) and aenigmatite. Trace amounts of apatite and zircon are present in many samples. For sample PC-06, an intrusion of quartz trachyte (~67.7 wt.% SiO_2), an Andersen and Lindsley (1988) two-oxide temperature and log fO_2 of 768 °C and −16.7 (FMQ-1.5) was determined.

3.2.3. Emory Peak Rhyolite Member (EPR)

The Emory Peak Rhyolite Member (Burro Mesa Rhyolite of Maxwell et al., 1967) consists of a series of quartz-bearing rhyolitic welded to rheomorphic ash-flow tuffs that erupted from intra- and extra-caldera postcaldera vents at 31.93±0.13 Ma (Barker et al., 1986; Miggins et al., 2004). Intrusive rocks petrographically and geochemically identical to the EPR form a series of east and northeast trending dikes that cross-cut the Chisos Group, PCR, and BRM. EPR samples studied consist of welded, devitrified ash-flow tuff and rheomorphic tuff, some of which have large (up to 10 cm), rounded inclusions of basalt similar to BMB. Sanidine (Or_{41}) and quartz are the dominant phenocrysts; minor phenocrysts include magnetite (Mgt_{53}), fluorian (2.21 wt.% F) biotite (annite), monazite, and zircon. Vapor-phase fluorian arfvedsonite (1.50 wt.% F) is a ubiquitous groundmass phase in the rheomorphic tuff. The presence of biotite in this assemblage suggests equilibration at low temperatures (<700 °C) under reducing conditions and close to H_2O saturation (Scaillet and Macdonald, 2001). For oxygen fugacities defined by the FMQ buffer, the assemblage annite+sanidine+magnetite is in equilibrium at 680–690 °C at ~1 kbar of total pressure (Dachs, 1994).

3.3. Burro Mesa Formation

Units in the Castolon graben include the Wasp Springs Tuff Member (WST) and the Burro Mesa Rhyolite Member (BUM), which erupted between 29.40±0.17 and 28.96±0.14 Ma (Miggins et al., 2004). The BUM includes aphyric comendite lava and ash-flow tuff (Lower Burro Mesa, LBM), and phyric comendite lava and ash-flow tuff (Upper Burro Mesa, UBM); on Burro Mesa, a mugearite lava flow similar to BMB lavas occurs between the LBM and UBM (Henry et al., 1989; Holt, 1998; Adams, 2004). Recent work in the Castolon area has demonstrated that outcrops of the BUM do not represent erosional remnants of EPR-correlative flows that originated in the Chisos Mountains, as stated by earlier workers (Maxwell et al., 1967; Ogley, 1978), but instead represent several individual lava dome volcanoes (Henry et al., 1989; Holt, 1998; Barker, 2000; Parker, 2002; Adams, 2004). We consider neither the WST nor the BUM to be part of the SRF; instead, these are included as informal members in the (new) Burro Mesa Formation, following Benker (2005).

4. Geochemistry

4.1. Classification

Samples of the South Rim Formation (SRF) and representative samples of Chisos Group mafic lavas (Henry and Davis, 1996; Adams, 2004) were classified using the total alkalis versus silica (TAS) diagram (Fig. 3; Le Maitre et al., 2002). Most SRF samples have an agpaitic index (A.I.=mol Na+K/Al) greater than unity and/or groundmass arfvedsonite or aenigmatite, which indicates that these rocks are peralkaline. The presence of arfvedsonite and/or aenigmatite in some rocks despite

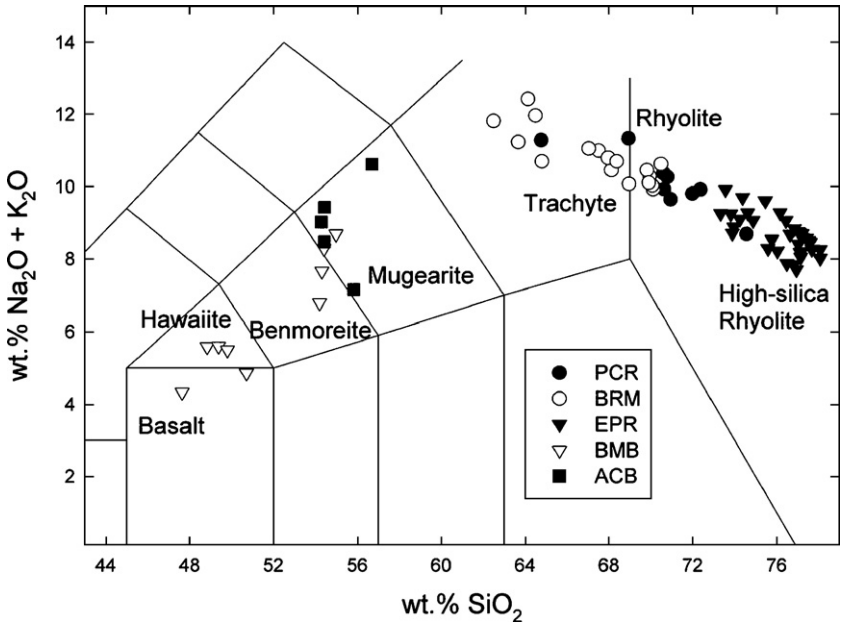

Fig. 3. South Rim Formation data from this report and Chisos Group data from Henry and Davis (1996) and Adams (2004) plotted on a total alkalis–silica (TAS) diagram (Le Maitre et al., 2002). Members of the South Rim Formation include the Pine Canyon Rhyolite Member (PCR), the Boot Rock Member (BRM), and the Emory Peak Rhyolite Member (EPR); representative formations of the Chisos Group include the Bee Mountain Basalt (BMB) and the Alamo Creek Basalt (ACB).

values of A.I. < 1.0 suggests that many of these samples have lost alkali components. The Pine Canyon Rhyolite (PCR) represents the most peralkaline unit (A.I. = 1.03–1.21) and most samples classify as rhyolite or comendite (borderline pantellerite). The Boot Rock Member (BRM) is less peralkaline (A.I. = 0.93–1.13) and most samples classify as quartz trachyte or comenditic trachyte and comendite. The Emory Peak Rhyolite (EPR) is the least peralkaline unit (A.I. = 0.89–1.09) and classifies as high-silica rhyolite or comendite. Chisos Group lavas plot between basalt (~45 wt.% SiO_2) and mugearite (~57 wt.% SiO_2), which results in a "Daly Gap" between Chisos Group and SRF suites.

Both the Pine Canyon suite and the Emory Peak suite can also be classified as A-type (anorogenic) magmas (Loiselle and Wones, 1979; Whalen et al., 1987). At ~70% SiO_2, the PCR has high total alkalis (9.5 wt.%), low CaO (0.50 wt.%), very high FeO^T/MgO (150), and elevated concentrations of high field-strength elements (HFSE) (e.g., 1850 ppm Zr, 225 ppm Nb). EPR is also characterized by high total alkalis (7–9 wt.%), low CaO (<0.50 wt.%), high FeO^T/MgO (up to 360), and somewhat elevated concentrations of HFSE (e.g., 700–900 ppm Zr, 100–150 ppm Nb). On tectonic discrimination diagrams (not presented), both suites plot in the Within Plate Granite (Y vs. Nb, Y+Nb vs. Rb; Pearce et al., 1984) and A-type fields (Zr vs. 10000 Ga/Al, FeO^T/MgO vs. Zr+Nb+Ce+Y; Whalen et al., 1987).

4.2. Pearce element ratio diagrams

Harker diagrams are not particularly useful for discriminating trends in these silicic rocks: all major-elements show a monotonous decline with increasing SiO_2 (Benker, 2005). Therefore, we instead present Pearce (1968) element ratio (PER) diagrams. PER diagrams are graphs of A/Ω vs. B/Ω, where A, B, and Ω are all compositional abundances, and Ω is a conserved, or incompatible, element. PER diagrams are based on the stoichiometry of rock-forming minerals, and slopes of data distributions are equal to the A:B ratio of minerals lost or gained during differentiation of a suite of cogenetic rocks (Russell and Nicholls, 1988). Representative PER diagrams that use Zr as the conserved-element denominator (following Bradshaw, 1992) are presented in Fig. 4. Two obvious suites within the South Rim Formation can be seen in these diagrams: one that includes the Pine Canyon Rhyolite (PCR), the Boot Rock Member (BRM), and the Lone Mountain (PJ-01) and Little Nugent (PC-06) intrusions (Pine Canyon suite); and another that includes the Emory Peak Rhyolite (EPR), and the Hayes Ridge (PC-05), K-Bar (KB-01), Panther Pass (PP-03), Appetite Peak (AP-

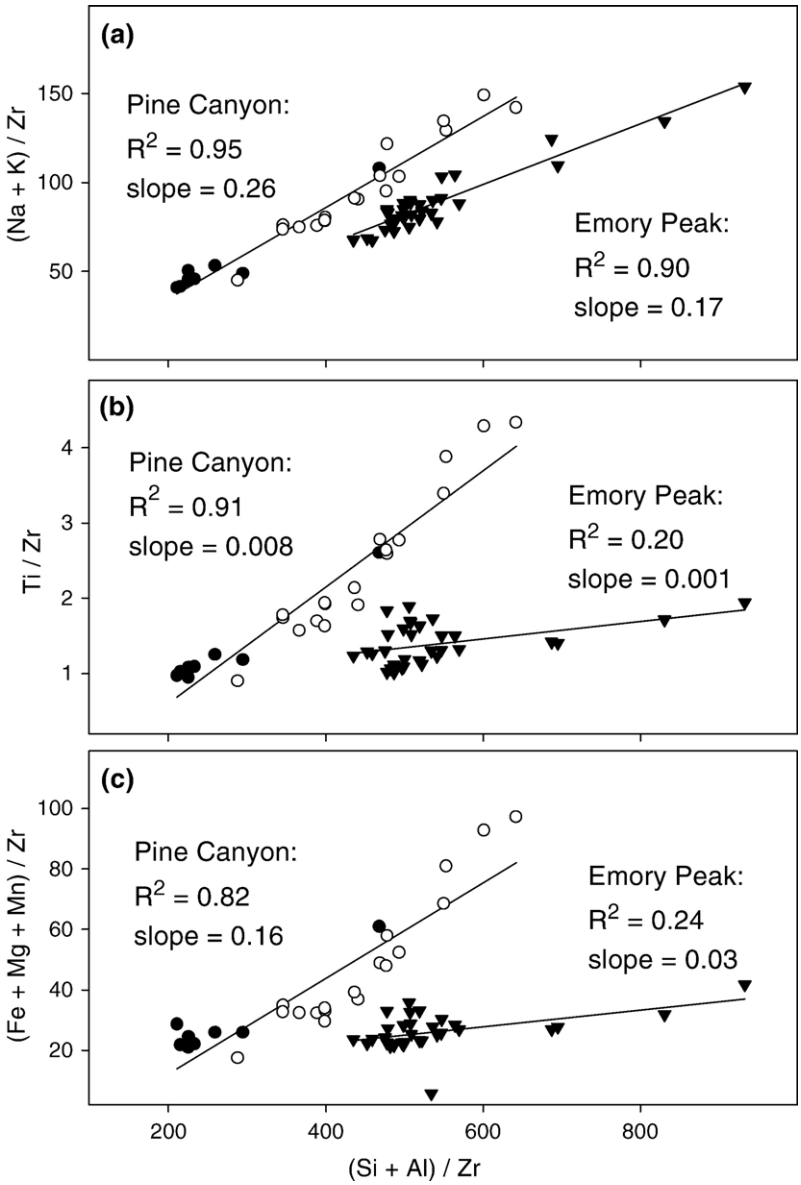

Fig. 4. Pearce (1968) element ratio (PER) diagrams for the South Rim Formation using Zr as the conserved-element denominator (Bradshaw, 1992). Symbols are the same as in Fig. 3.

01), and Lost Mine Trail (LM-02) intrusions (Emory Peak suite).

It can be inferred from the PER diagrams that it is unlikely that the high-silica rhyolite Emory Peak suite evolved via fractional crystallization from the Pine Canyon suite. However, closed system processes may be able to explain compositional variation within each suite. The Pine Canyon suite demonstrates an increase in SiO_2 from ~62 to ~72 wt.% with a decrease in (Si + Al)/Zr and all major element oxides (Benker, 2005). The similarity between the calculated (Stanley and Russell, 1990) alkali feldspar fractionation slope (0.25) and observed slope (0.26) in Fig. 4a, coupled with the dominant presence of alkali feldspar as a phyric phase in these rocks, strongly suggests that fractional crystallization of an assemblage dominated by alkali feldspar with minor clinopyroxene and Fe–Ti oxides (Fig. 4b,c) played a dominant role in the petrogenesis of the quartz trachyte–rhyolite suite. There is much less systematic variation in the Emory Peak suite, especially with respect to Fe, Mg, Mn, and Ti, which may be due to the crystallization of zircon, an accessory phase observed in

the EPR. Only the alkali metals strongly correlate with silicon and aluminum, declining with a slope of 0.17, which would be consistent with fractional crystallization of an assemblage of quartz and alkali feldspar.

4.3. Trace-element geochemistry

Trace element variation diagrams are presented in Fig. 5, which use Nb as a differentiation index. Despite being higher in silica, the Emory Peak suite is depleted in all incompatible trace elements compared to the Pine Canyon suite, and with the exception of Ga there is little obvious systematic variation within the Emory Peak suite. Systematic variation is observed within the Pine Canyon suite: with increasing Nb, all incompatible trace elements exhibit an approximately three-fold increase in concentration, Sr declines from 13 to 7 ppm, and Ba declines from 106 to 9 ppm. Incompatible trace-element ratios vary between each suite, but remain fairly constant within suites: for example, Zr/Hf is 40.6±2.0 for the Pine Canyon suite and 32.1±3.8 for the Emory Peak suite, and Rb/Nb is

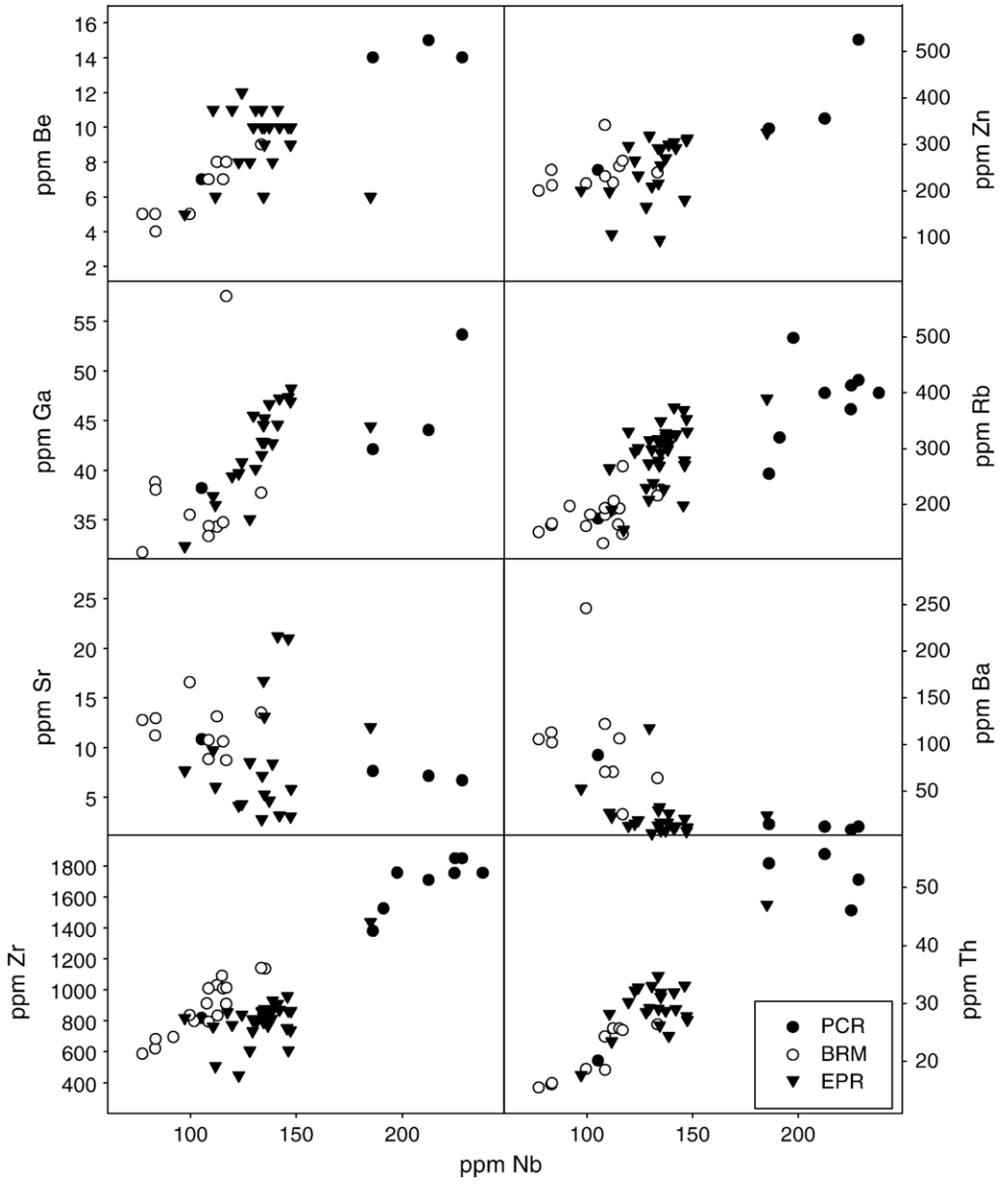

Fig. 5. Trace-element variation diagrams for the South Rim Formation using Nb as a differentiation index. Symbols are the same as in Fig. 3.

1.7±0.2 (Pine Canyon suite) and 2.2±0.6 (Emory Peak). For comparison, incompatible trace element ratios for the Bee Mountain Basalt (Henry and Davis, 1996; Adams, 2004) are 41.5±2.0 (Zr/Hf) and 1.45±0.48 (Rb/Nb).

REE plots of representative analyses (normalized following Boynton, 1984) are presented in Fig. 6. Again despite being higher in silica, the Emory Peak suite is depleted in REE compared to the Pine Canyon suite: Ce is enriched by 210–754× chondrite in the Pine Canyon suite compared to 43–439× chondrite in the Emory Peak suite, and Yb is enriched by 26–76× chondrite in the Pine Canyon suite versus 30–83× chondrite in the Emory Peak suite. Chondrite-normalized values for Ce/Yb and La/Sm remain fairly constant within the Pine Canyon suite at 8.0±0.4 and 4.2±0.3, respectively

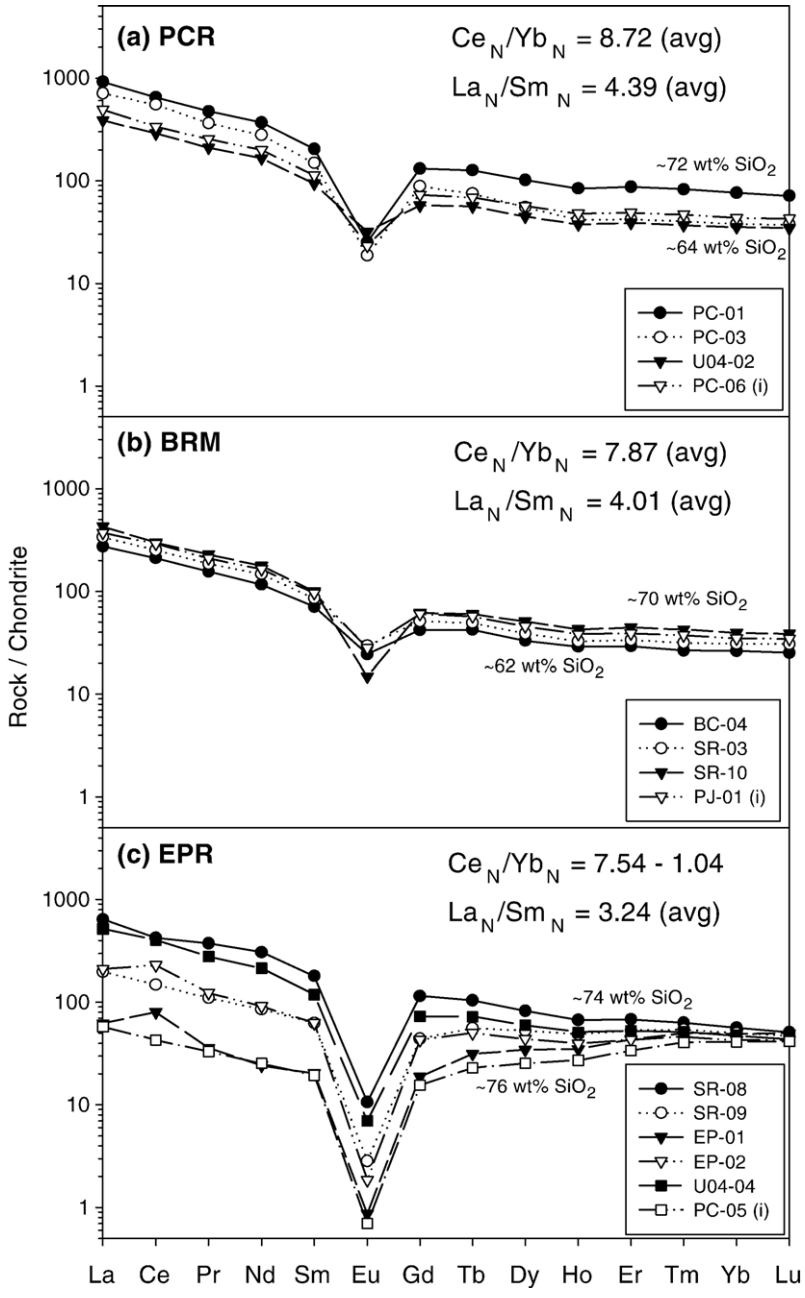

Fig. 6. Rare-earth element diagrams for representative samples from (a) the Pine Canyon Rhyolite Member, (b) the Boot Rock Member, and (c) the Emory Peak Rhyolite Member. All rock samples are normalized to chondrite following Boynton (1984).

(although Ce_N/Yb_N does jump to 10.8 and 14.1 in two higher-silica samples of PCR). Within the Emory Peak suite, La_N/Sm_N is lower, but fairly constant, at 3.2±0.5, whereas Ce_N/Yb_N systematically decreases from 7.5 to 1.0 with increasing whole-rock silica. Both suites have a negative Eu anomaly that deepens with increasing silica: within the Pine Canyon suite, Eu/Eu∗ decreases from 0.45 to 0.15, and within the Emory Peak suite, Eu/Eu* decreases from 0.31 to 0.03. For comparison, normalized rare earth element ratios for the Bee Mountains Basalts (Henry and Davis, 1996; Adams, 2004) are 7.1± 1.3 (Ce_N/Yb_N), 3.0±0.9 (La_N/Sm_N), and 1.1 to 0.8 (Eu/Eu*).

The trace-element data clearly indicate that the high-silica rhyolite of the Emory Peak suite is not related to the quartz trachyte and rhyolite of the Pine Canyon suite via fractional crystallization processes, although fractional crystallization processes may be responsible for variation within the individual suites.

5. Petrogenesis

5.1. Origin of quartz trachyte via assimilation and fractional crystallization (AFC) of alkali basalt

Major-element mass balance models (Bryan et al., 1969) can both test the hypotheses suggested by PER diagram analysis as well as quantify the relative proportion of the various phases involved during petrogenesis, which can be tested against both the petrography and the trace element data. Major-element mass balance models are presented (Table 1) that test fractional crystallization hypotheses for the origin of quartz trachyte from basalt (Stage 1), and the origin of rhyolite from quartz trachyte (Stage 2). Major-element models suggests that the most primitive perakaline quartz trachyte of Boot Rock Member presented in this report (BC-04) could be derived via 81% fractional crystallization ($F=0.19$) of an assemblage of plagioclase,

Table 1
Quartz trachyte–rhyolite major-element mass balance models

	Parent	Daughter						Parent	
Stage 1 FC	H90-50	BC-04	Pl	Cpx	Mgt	Ol	Ap	Calc.	Residuals
SiO_2	47.65	64.81	54.52	51.81	0.00	38.10	0.00	47.67	−0.02
TiO_2	2.51	0.43	0.00	1.01	26.49	0.00	0.00	2.88	−0.37
Al_2O_3	17.03	14.44	28.26	1.65	2.31	0.00	0.00	17.03	0.00
FeO^T	12.72	7.20	0.00	9.02	68.46	24.59	0.22	12.57	0.15
MnO	–	–	–	–	–	–	–	–	–
MgO	6.50	0.08	0.00	13.37	2.74	37.32	0.57	6.58	−0.08
CaO	8.62	2.15	12.63	21.85	0.00	0.00	55.67	8.57	0.05
Na_2O	3.35	5.52	4.41	0.68	0.00	0.00	0.00	3.25	0.10
K_2O	0.98	5.18	0.18	0.00	0.00	0.00	0.00	1.05	−0.07
P_2O_5	0.45	0.06	0.00	0.00	0.00	0.00	43.54	0.51	−0.06
		F						100.11	0.188
	Results:	0.185	0.496	0.059	0.104	0.147	0.011		$=\Sigma r^2$
	Normalized:		0.607	0.072	0.127	0.180	0.014		
Stage 2 FC	BC-04	PC-01	Kfs	Cpx	Ilm	Ol	Ap	Calc.	Residuals
SiO_2	64.81	72.39	66.35	47.41	0.03	28.65	0.00	64.81	0.00
TiO_2	0.43	0.32	0.00	0.52	50.74	0.12	0.00	0.43	0.00
Al_2O_3	14.44	11.67	19.17	0.49	0.00	0.00	0.00	14.38	0.06
FeO^T	7.20	5.12	0.20	30.62	47.69	65.73	0.22	7.19	0.01
MnO	0.13	0.10	0.00	0.99	1.45	3.99	1.59	0.28	−0.15
MgO	0.08	0.00	0.00	0.30	0.02	1.06	0.56	0.07	0.02
CaO	2.15	0.51	0.35	19.17	0.04	0.43	54.78	2.16	−0.01
Na_2O	5.52	5.24	7.11	0.49	0.01	0.01	0.00	5.64	−0.12
K_2O	5.18	4.63	6.83	0.01	0.02	0.01	0.00	5.26	−0.08
P_2O_5	0.06	0.02	0.00	0.00	0.00	0.00	42.84	0.04	0.02
		F						100.26	0.047
	Results:	0.306	0.562	0.006	0.001	0.091	0.037		$=\Sigma r^2$
	Normalized:		0.806	0.008	0.001	0.131	0.054		

Analysis H90-50 (alkali basalt) adopted from Henry and Davis (1996).
Key to minerals: Pl, plagioclase feldspar; Kfs, alkali feldspar; Ol, olivine; Cpx, clinopyroxene; Mgt, magnetite; Ilm, ilmenite; Qtz, quartz; Ap, apatite. Stage 1 mineral analyses adopted from Schucker (1986) and Nelson et al. (1987). Stage 2 olivine analysis adopted from White et al. (2005), apatite from Deer et al. (1966), all others are from this report. Other symbols: F=liquid fraction; Σr^2=sum of squares of residuals.

clinopyroxene, olivine, magnetite, and apatite from alkali basalt (H90-50; Henry and Davis, 1996). The sum of the squares of the residuals (Σr^2) for this model is acceptable (0.188). This major-element mass balance models is consistent with petrography and mineralogy (Schucker, 1986).

An origin of quartz trachyte via fractional crystallization of alkali basalt is supported by major-element mass balance modelling and some similar incompatible trace element ratios (e.g., Zr/Hf, Ce/Yb). However, there is also trace element evidence that suggests that fractional crystallization alone cannot explain the origin of quartz trachyte, and that open-system processes must also have played a role: (1) incompatible trace-element concentrations (including Nb, Rb, Th, Zr, Hf, and REE) in the most differentiated Chisos Group mafic lavas (~57 wt.% SiO_2) are similar to those in the least differentiated South Rim Formation quartz trachyte lavas (~62 wt.% SiO_2), which suggests assimilation of wall-rock depleted with respect to these elements; and (2) K/Rb values for the model parent (H90-50, K/Rb=678) are much higher than for the model daughter (BC-04, K/Rb=286), which argues against fractional crystallization and recommends assimilation of low-K/Rb wall-rock.

DePaolo's (1981) equation for modelling trace-element behavior during combined assimilation and fractional crystallization (AFC) is used to test this hypothesis. Bulk partition coefficients were calculated using minerals and mineral proportions determined by major-element mass balance modelling (see Table 1, Stage 1) and mineral/melt partition coefficients from Paster et al. (1974), Villemant et al. (1981), McKenzie and O'Nions (1991), and Pearce and Norry (1979). The same model parent (H90-50; Henry and Davis, 1996) and daughter (BC-04) magmas used for major-element mass balance modelling was used for trace element AFC modelling. An estimate of average Phanerozoic shale from Condie (1993) was selected as the model assimilant. Shale is considered to be a very likely assimilant because the Big Bend area developed on accreted Phanerozoic crust that includes thick flysch sequences (Cameron et al., 1992; James and Henry, 1993). Model results and calculated bulk partition coefficients are presented in Fig. 7 for (a) M_a/M_c (mass assimilated/mass crystallized)=0.3 and (b) M_a/M_c=0.4. These results are arranged and normalized on a spider diagram following Thompson (1982) and show that quartz trachyte may have evolved from alkali basalt via 60–70% crystallization (F=0.4–0.3) of an assemblage of plagioclase, clinopyroxene, olivine, magnetite, and apatite coupled with assimilation (M_a/M_c=0.3 to 0.4) of shale wall-rock. However, there are major discrepancies at each of the compatible elements (especially Ba and Sr), where model results are much higher than the model daughter, which may be due to either too-low partition coefficients (e.g., D_{Ba}=2.7 and D_{Sr}=5.0 would result in a better fit, which could suggest a greater role for plagioclase, and a possible role for alkali feldspar, amphibole, and/or biotite), too-high concentrations in the model assimilant, or a combination of these two possibilities.

5.2. Origin of the quartz trachyte–rhyolite suite via fractional crystallization

Major element mass balance modelling (Table 1, Stage 2) suggests that the differentiation of quartz trachyte (BC-04) to peralkaline rhyolite (PC-01) can be explained by 69% fractional crystallization (F=0.31) of an assemblage dominated by alkali feldspar (80.6%) with clinopyroxene, ilmenite, fayalite, and apatite. The Σr^2 for this model is 0.047. Major element model results are consistent with observed petrography and mineralogy, major-element trends shown on the PER diagrams, and incompatible trace element ratios. The fractional crystallization hypothesis is tested with trace element modelling (e.g., Allègre et al., 1977). Bulk partition coefficients were calculated using minerals and mineral proportions determined by major-element mass balance modelling, plus a trace amount (0.0001) of zircon, which was observed as a minor phase in some samples, and mineral/melt partition coefficients from Paster et al. (1974), Pearce and Norry (1979), Fujimaki (1986), Villemant (1988), White (2003), and White et al. (2003).

Unlike most trace-elements that have alkali feldspar/melt partition coefficient that do not vary significantly during differentiation of the quartz trachyte to rhyolite suite, Europium gradually changes from a compatible element (D_{Eu}=1.36) in alkali feldspar in the model parent (BC-04) to an incompatible element (D_{Eu}=0.65) in the model daughter (PC-01), as estimated using the method (Model Eu-A) described by White (2003). Bulk partition coefficients for samples BC-04 (1.34) and PC-01 (0.78) were calculated using the estimated partition coefficients for alkali feldspar, partition coefficients for clinopyroxene (1.60), ilmenite (0.74), and fayalite (0.02) from Villemant (1988), and apatite (30.0) from Mahood and Stimac (1990), and the model results presented in Table 1 (Stage 2). From these bulk partition coefficients and the value of F for the model daughter predicted by the major element model (0.306), a linear

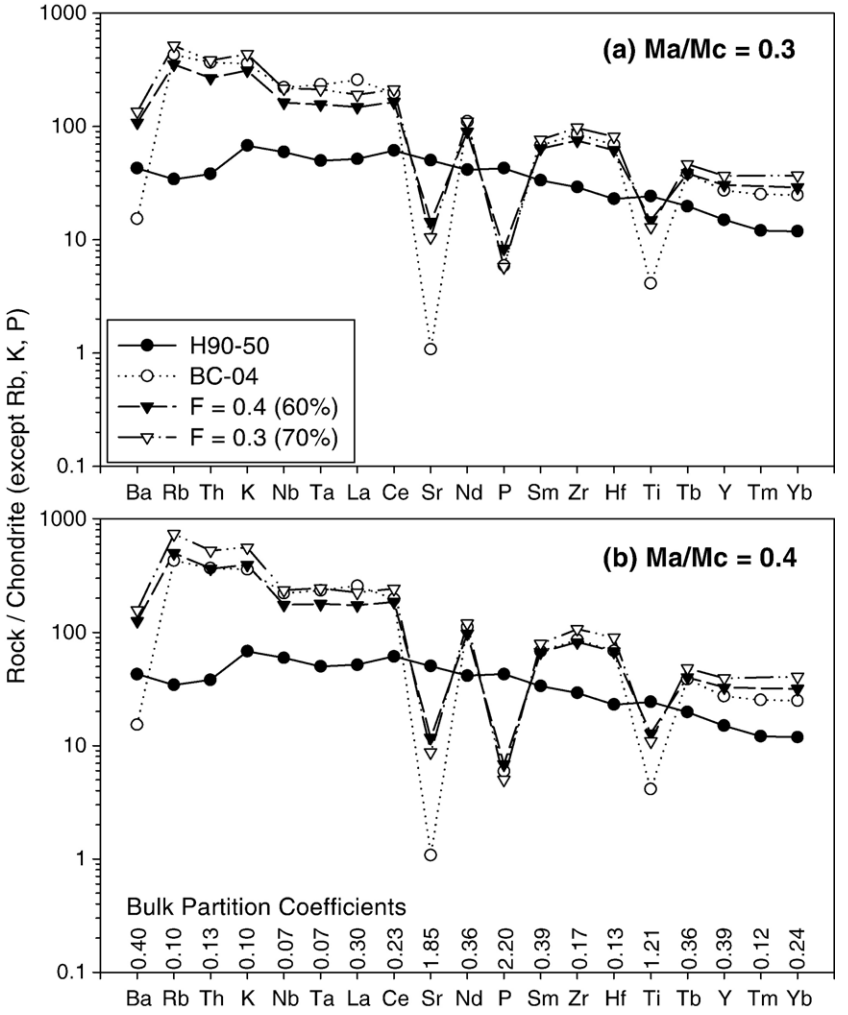

Fig. 7. Results of assimilation–fractional crystallization (AFC) modelling (DePaolo, 1981) of the origin of quartz trachyte (BC-04, ~64 wt.% SiO_2) from alkali basalt (H90-50, ~48 wt.% SiO_2) with mass assimilated / mass crystallized (M_a/M_c) ratios of (a) 0.3 or (b) 0.4. Model results are plotted on a spider diagram arranged and normalized following Thompson (1982). The model assimilant is average Phanerozoic shale (Condie, 1993). Bulk partition coefficients were calculated using mineral proportions calculated by major-element mass balance modelling (see Table 1, Stage 1) and mineral/melt partition coefficients from Paster et al. (1974), Pearce and Norry (1979), Villemant et al. (1981), and McKenzie and O'Nions (1991).

equation describing bulk D(Eu) as a function of F is calculated:

$$D(\mathrm{Eu}) = 0.5266 + 0.8193(F).$$

Greenland (1970) derived an equation for Rayleigh fractional crystallization for a bulk partition coefficient that varies linearly with F, expressed as $D = a + bF$:

$$\ln C_L/C_O = (a-1)\ln F + b(F-1),$$

and this equation is used to model the behavior of Eu.

Model results and calculated bulk partition coefficients are presented in Fig. 8 for representative trace elements (Rb, Sr, Zr, Ba, Ce, Eu, Yb, and Th) plotted versus Nb. Trace element models predict that the model daughter (PC-01) would be produced after ~75% crystallization of the model parent (BC-04), which is similar to the amount predicted (~70%) by major-element modelling. These results are combined with the results of AFC modelling of the origin of the quartz trachyte from alkali basalt in Fig. 9, a plot of K/Rb versus Rb. It is very probable that fractional crystallization of the observed assemblage (alkali feldspar, clinopyroxene, fayalite, ilmenite, apatite, and zircon) following protracted AFC of alkali basalt is the petrogenetic mechanism responsible for the chemical variation in the Boot Rock and Pine Canyon Rhyolite Members. These model results for the petrogenesis of

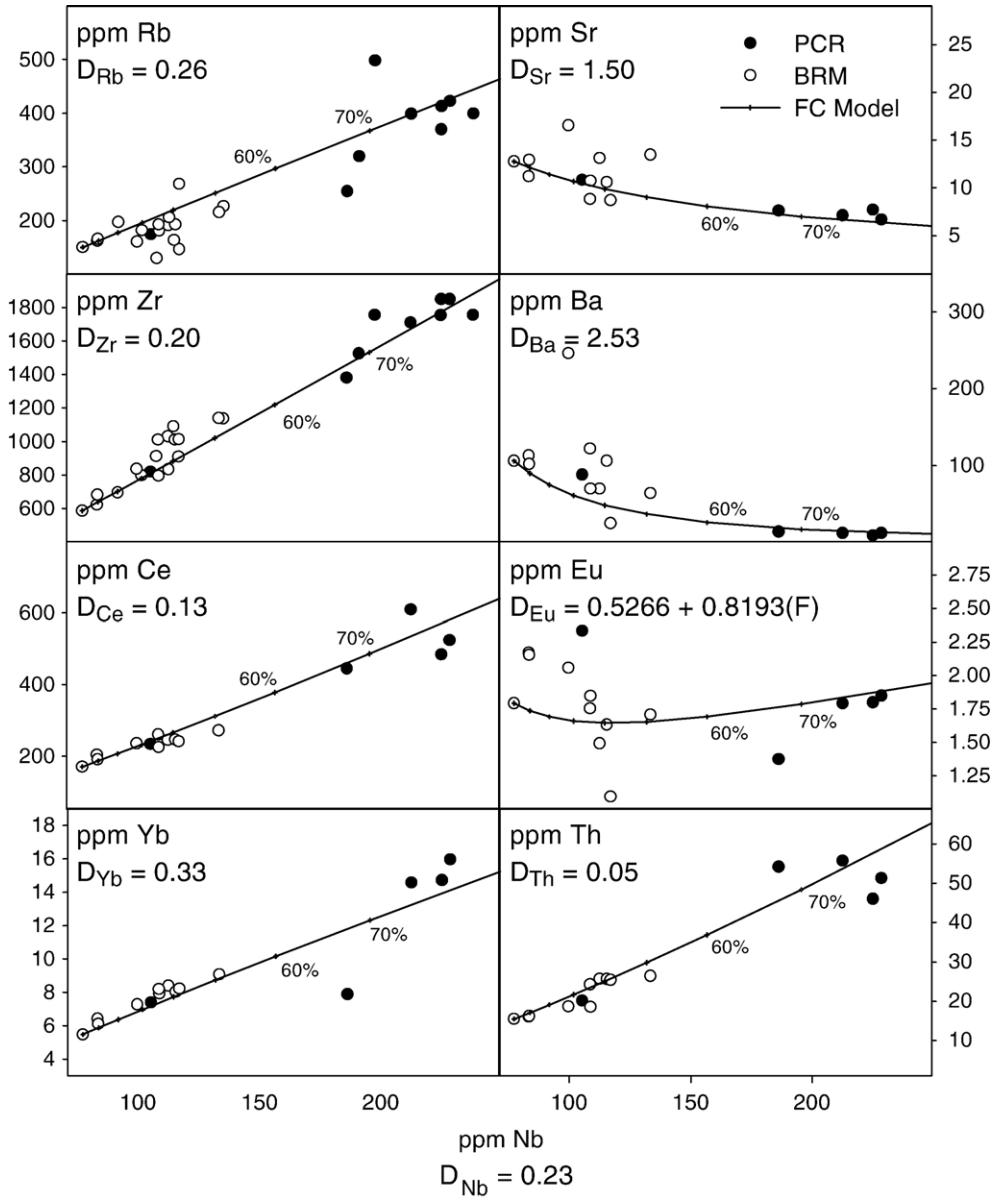

Fig. 8. Results of fractional crystallization (FC) modelling of the origin of rhyolite (PC-01, ~72 wt.% SiO_2) from quartz trachyte (BC-04, ~64 wt.% SiO_2) for representative trace elements. Bulk partition coefficients were calculated using mineral proportions calculated by major-element mass balance modelling (Table 1, Stage 2) and mineral/melt partition coefficients from Paster et al. (1974), Pearce and Norry (1979), Fujimaki (1986), Villemant (1988), White (2003), and White et al. (2003). Symbols are the same as in Fig. 3.

the Pine Canyon quartz trachyte–rhyolite suite are similar to those described by Peccerillo et al. (2003) for the peralkaline rocks from the Quaternary Gedemsa volcano in the Central Ethiopian Rift: they showed that trachyte could evolve from basalt following ~70% fractional crystallization plus moderate assimilation, and that peralkaline rhyolite could evolve from trachyte following ~50–60% fractional crystallization with small rates of assimilation.

5.3. Origin of high-silica rhyolite by crustal melting, volatile enrichment, and fractional crystallization

There is strong evidence that indicates that the EPR high-silica rhyolite is not related to the BRM and PCR quartz trachyte–rhyolite suite by fractional crystallization processes: (1) PER diagrams suggest that the high-silica rhyolite forms a liquid line of decent distinct from the quartz trachyte–rhyolite suite, (2) high-silica

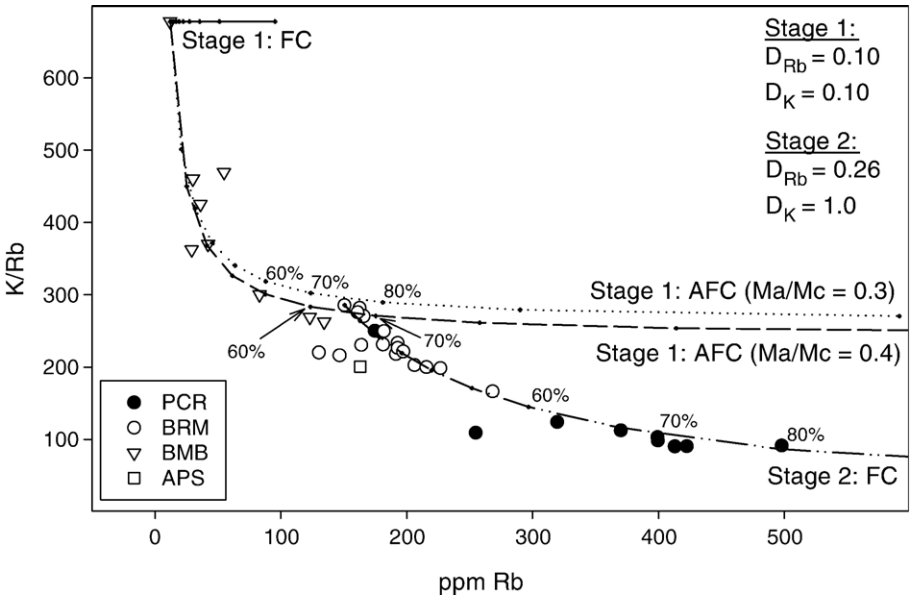

Fig. 9. Plot of K/Rb versus Rb showing the combined results of Stage 1 (AFC) and Stage 2 (FC) modelling. Symbols are the same as in Fig. 3, plus APS, average phanerozoic shale (Condie, 1993).

rhyolite is depleted in incompatible elements (including Be, Zn, Ga, Rb, Y, Zr, Th, and REE) with respect to quartz trachyte and low-silica rhyolite; and (3) high-silica rhyolite has lower Zr/Hf and Zr/Nb ratios than the quartz trachyte–rhyolite suite. Since quartz trachyte and rhyolite must be excluded as possible parental magmas, models of crustal anatexis for the origin of the Emory Peak suite are evaluated.

BBNP is underlain by Phanerozoic crust accreted during the late Paleozoic Marathon–Oucachita orogeny (James and Henry, 1993). This crust consists primarily of allochthonous, Cambrian to Pennsylvanian clastic sedimentary rocks that have undergone low-grade regional metamorphism, and have been locally modified by middle Tertiary magmatism. Evidence from xenoliths at La Olivina, Chihuahua, México, show that deep crust in this terrane consists of paragneisses, interpreted to represent metamorphic Carboniferous flysch deposits; intermediate- to silicic-orthogneisses, interpreted to represent fragments of accreted Precambrian continental crust; and mafic granulites, interpreted to represent middle Tertiary olivine-rich gabbroic cummulates (Cameron et al., 1992).

It is unlikely that the peralkaline Emory Peak Rhyolite was generated by partial melting of alkali-poor and alumina-rich sedimentary or metasedimentary rocks; therefore, the most likely source rock would be either igneous or metaigneous. Equilibrium batch melting (EBM) is tested first with major element mass balance modelling (Table 2, Stage 3); the model source rock is a trace-element depleted deep crustal (<25 km) mafic granulite (MN32) adopted from Cameron et al. (1992). Major-element modelling suggests that the most primitive high-silica rhyolite melt (SR-08) can be produced with 4.1% partial melting of mafic granulite with a residual assemblage of approximately 50% plagioclase, 21% clinopyroxene, 12% orthopyroxene, 16% magnetite, and 1% apatite. This model has an acceptable Σr^2 of 0.370.

The EBM hypothesis is further tested with trace-element modelling (e.g., Minster and Allègre, 1978) (Fig. 10). Mineral proportions used to calculate bulk partition coefficients for the mafic granulite were adopted from Cameron et al. (1992): 42% plagioclase, 23% clinopyroxene, 28% orthopyroxene, and 7% Fe–Ti oxide. Mineral/melt partition coefficients were adopted from Schnetzler and Philpotts (1970), Paster et al. (1974), McKenzie and O'Nions (1991), and Sobolev et al. (1996). These results suggest that it may be possible to produce the least silicic sample of EPR (SR-08) with ~5% partial melting of mafic granulite. However, the predicted negative anomaly at Eu is not deep enough; this may be due to either residual plagioclase in the source during melting, a source rock with lower Eu, or a need for larger plagioclase/melt partition coefficients.

Model concentrations of other incompatible elements show an interesting decoupling: for a 5% partial melt of mafic granulite, predicted values for Nb (127 ppm), Y (156 ppm), and Zr (882 ppm) are close to SR-08 (135 ppm Nb, 123 ppm Y, and 829 ppm Zr), but

Table 2
High-silica rhyolite major-element mass balance models

	Source	Melt						Source	
Stage 3 EBM	MN32	SR-08	Pl	Cpx	En	Mgt	Ap	Calc.	Residuals
SiO_2	46.60	74.87	54.52	51.81	58.48	0.00	0.00	46.62	−0.02
TiO_2	3.72	0.22	0.00	1.01	0.00	26.49	0.00	4.25	−0.53
Al_2O3	15.00	12.25	28.26	1.65	0.88	2.31	0.00	14.99	0.01
FeO^T	13.12	2.99	0.00	9.02	4.73	68.46	0.22	12.92	0.20
MnO	–	–	–	–	–	–	–	–	–
MgO	7.00	0.01	0.00	13.37	34.71	2.74	0.57	6.99	0.01
CaO	11.10	0.29	12.63	21.85	0.50	0.00	55.67	11.12	−0.02
Na_2O	2.70	4.26	4.41	0.68	0.23	0.00	0.00	2.48	0.22
K_2O	0.29	5.04	0.18	0.00	0.08	0.00	0.00	0.31	−0.02
P_2O_5	0.37	0.02	0.00	0.00	0.00	0.00	43.54	0.34	0.03
		F						100.01	0.370
	Results:	0.041	0.484	0.206	0.110	0.152	0.008		$=\Sigma r^2$
	Normalized:		0.504	0.214	0.115	0.158	0.008		

	Parent	Daughter					Parent	
Stage 4 FC	SR-08	EP-01	Kfs	Qtz	Bt	Mgt	Calc.	Residuals
SiO_2	74.87	78.29	66.07	100.00	35.51	0.17	74.87	0.00
TiO_2	0.22	0.16	0.00	0.00	3.66	15.27	0.25	−0.03
Al_2O_3	12.25	10.60	18.84	0.00	5.55	0.06	12.22	0.04
FeO^T	2.99	2.53	0.26	0.00	38.40	74.03	2.99	0.01
MnO	0.03	0.03	0.00	0.00	0.54	0.43	0.03	0.00
MgO	0.01	0.01	0.00	0.00	0.02	0.00	0.01	0.00
CaO	0.29	0.07	0.01	0.00	0.13	0.04	0.05	0.24
Na_2O	4.26	3.87	6.61	0.00	0.12	0.03	4.33	−0.06
K_2O	5.04	4.42	7.17	0.00	8.61	0.01	5.08	−0.04
P_2O_5	0.02	0.02	0.00	0.00	0.00	0.00	0.01	0.01
		F					99.84	0.067
	Results:	0.638	0.281	0.053	0.029	0.003		$=\Sigma r^2$
	Normalized:		0.769	0.146	0.079	0.007		

Analysis MN32 (mafic granulite) adopted from Cameron et al. (1992).
Key to minerals: Pl, plagioclase feldspar; Kfs, alkali feldspar; Ol, olivine; Cpx, clinopyroxene; Mgt, magnetite; En, Enstatite; Bt, biotite; Qtz, quartz; Ap, apatite. Stage 3 mineral analyses adopted from Schucker (1986), Nelson et al. (1987), and Deer et al. (1966); all others are from this report. Other symbols: F = liquid fraction; Σr^2 = sum of squares of residuals.

predicted values for Rb (34 ppm) are much lower than SR-08 (292 ppm Rb). The inconsistency of Rb concentrations with a mineral–melt differentiation model such as EBM may suggest a role for volatile enrichment in the origin of the high-silica rhyolite. Several previous workers have suggested that metal cations may form complexes with specific halogens: Bailey and Macdonald (1975) described strong linear correlations for Cl–Nb–Y and F–Zr–Rb, although others (e.g., Hildreth, 1981) have suggested that Zr complexes with Cl. The presence of high-F biotite and vapor-phase arfvedsonite in the EPR shows this component was present in the magma, and may be responsible for Rb-enrichment of the EPR. If this interpretation is valid, then it is likely that the high-silica rhyolite formed by a small degree (~4–5%) of partial melting of a mafic granulite under the fluxing influence of fluorine. In the Rio Grande rift in southern New Mexico, young (<10 Ma) hydrothermal deposits closely related to asthenosphere-derived basalts have characteristically high concentrations of fluorine, probably derived from these basalts (Lueth et al., 2005). The origin of alkaline rocks via crustal anatexis was proposed by Bailey (1974), and has also been used to explain the origin of peralkaline magmas in the Kenya rift, including high-silica rhyolite at the Naivasha complex (Macdonald et al., 1987; Davies and Macdonald, 1987) and plateau-type flood phonolites (Hay and Wendlandt, 1995; Hay et al., 1995a,b). Unfortunately, at this time it is not possible to qualitatively test models of volatile enrichment; likewise, experimental evidence for the generation of peralkaline magmas from crustal anatexis is lacking (Scaillet and Macdonald, 2003).

A major-element mass balance model of fractional crystallization for variation within the EPR is presented in Table 2 (Stage 4). Variation within the high-silica

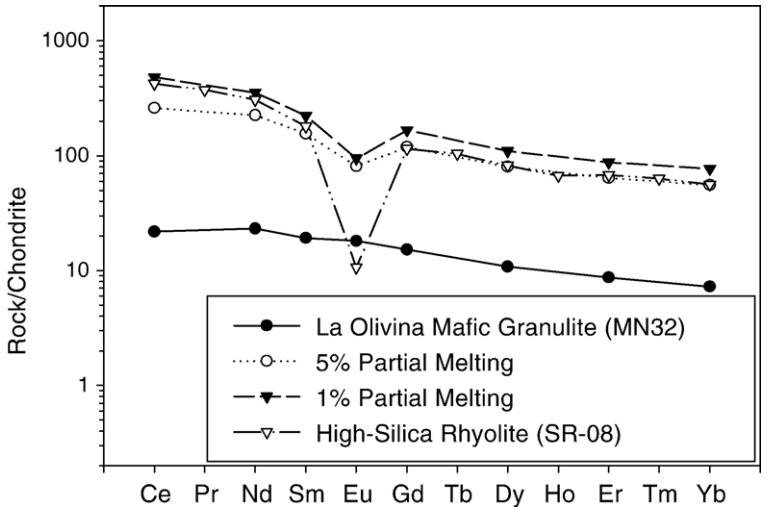

Fig. 10. Results of modal equilibrium batch melting (EBM) modelling of the origin of high-silica rhyolite (SR-08, ~74% SiO_2) from mafic granulite (MN32, Cameron et al., 1992).

rhyolite suite from 74.8 to 78.3 wt.% SiO_2 (SR-08 to EP-01) can be explained by 36% fractional crystallization (F=0.64) of an assemblage dominated by alkali feldspar (77%) and quartz (15%) with subordinate biotite and magnetite; this is consistent with petrography, mineralogy, and PER diagram analysis. The Σr^2 for this model is 0.067. Minor- and trace-element data suggest that, in addition to alkali feldspar and quartz, accessory minerals (monazite and zircon) have a dominant role in differentiation of this suite. From SR-08 to EP-01, P_2O_5 stays constant (~0.02 wt.%), Ce_N/Yb_N falls from 7.5 to 1.0 (see Fig. 6), Th/U drops from 3.2 to 2.3 due to the near-steady state behavior of Th (32 to 28 ppm), and both Zr (828 to 739 ppm) and Hf (25 to 22 ppm) also demonstrate near-steady state behavior. Monazite fractionation is evidenced by petrography and a progressive "flattening" of the REE pattern (Wark and Miller, 1993; Bea et al., 1994). Steady state behavior of P and Th, both of which are essential structural constituents (ESC) of monazite, suggest that the melt was saturated with respect to monazite throughout differentiation; similarly, steady state behavior of Zr and Hf (ESCs for zircon) in the suite suggest that the high-silica rhyolite was saturated with respect to zircon (Evans and Hanson, 1993).

6. Tectonic setting

Barker (1977) interpreted the TPMP to be the result of intraplate extension analogous with the Kenya Rift based primarily on petrology (voluminous outcrops of metaluminous to peralkaine quartz trachyte and rhyolite) and structural setting (normal faulting). Other workers suggested TPMP magmatism prior to 31 Ma was the result of subduction-related, continental arc volcanism instead of intraplate extension, based on the age of normal faults (<24 Ma) in the Trans-Pecos (Henry and Price, 1986); paleostress analysis of orientations of dikes and veins, which were interpreted to suggest a compressional stress regime until 31 Ma (Henry et al., 1991); and the different trace element ratios of basalts erupted before and after 31 Ma (James and Henry, 1991). This interpretation of the tectonic history of the TPMP is also consistent with space-time patterns of continental arc migration in the western USA and México (e.g., Coney and Reynolds, 1977).

However, the onset of magmatism prior to faulting by a few million years does not preclude an extensional origin for the magmas: in the southern Ethiopian segment of the East African Rift system, volcanism preceded faulting by ~20 Ma, and in northern Kenya volcanism began about 33 Ma and faulting began about 25 Ma (Ebinger et al., 2000). It is worth noting that volcanism at Pine Canyon began about 33 Ma while faulting in the Big Bend began between 28 and 23 Ma (Dickerson and Muehlberger, 1994). Additionally, paleostress analysis of dikes and veins does not provide a unique solution; although Henry et al. (1991) interpreted the orientation of maximum principal stress (σ_1) in pre-31 Ma structures to be east-northeast and thus perpendicular to the late Cretaceous–early Tertiary paleotrench, they note (p. 13, 551) that σ_1 could range between east-northeast and vertical, which would be

consistent with north-northwest extension. They also note (p. 13, 552) that there is considerable scatter in the orientation of dikes and veins, which indicates a small difference in magnitude between σ_1 and the minimum principal stress (σ_3) typical of tectonically inactive regions. Thus, it may be valid to characterize pre-31 Ma stresses in the TPMP as near-neutral, which is how Chapin et al. (2004) characterize the regional stress field between 45 and 36 Ma in New Mexico and Colorado. Finally, metasomatism of the mantle by slab-derived fluids during earlier an earlier phase of subduction could result in arc-like trace-element signatures in basalts that are clearly erupted in a continental rift (e.g., the Pliocene Taos Plateau Volcanic Field, northern Rio Grande rift, New Mexico: Dungan et al., 1986).

Structural and petrologic evidence from New Mexico and central Colorado suggest that a weakly compressional, near-neutral stress field persisted from 45 to 36 Ma, and that extension began in the region by 36 Ma (Lawton and McMillan, 1999; McMillan et al., 2000; Chapin et al., 2004; McIntosh and Chapin, 2004). These ages are consistent with plate motion evidence for a decrease in the rate of subduction at 43 Ma, and the onset of transtensional extension related to the formation of the Sierra Madre Occidental in northern México at 36–34 Ma (Ward, 1991). The petrology and petrogenesis of the Pine Canyon caldera is also consistent with development in a neutral or extensional, rather than compressional, stress field: the petrogenetic mechanisms described for the origin of the South Rim Formation are more consistent with those operating in extensional environments, such as the East African Rift system (e.g., Macdonald et al., 1987; Peccerillo et al., 2003), rather than compressional environments (cf. Eichelberger, 1978); these are A-type magmas with major- and trace-element signatures consistent with continental rifting (Martin, 2006-this volume); and ascent of viscous high-silica rhyolite from deep crust would be facilitated in an extensional regime and inhibited in a compressional one.

We suggest that the model for post-collisional and post-orogenic magmatism summarized by Bonin (2004) might be the best to use to describe the tectonic history of the TPMP:

(1) Collision ("Normal Subducton" phase of Lawton and McMillan, 1999). Flat-slab subduction of the Laramide plate from 100 to 45 Ma resulted in lithosphere stacking and orogenic growth, and was less favorable for magma ascent, as evidenced by a paucity of pre-45 Ma volcanic rocks in Trans-Pecos Texas (Henry and McDowell, 1986) and southern New Mexico (Chapin et al., 2004).

(2) Post-collision or late orogenic ("Early Slab Retreat" phase of Lawton and McMillan, 1999). A "relaxation" phase followed roll-back or break-off of the subducting slab from 45 to 36–34 Ma, which resulted in asthenospheric upwelling, partial melting of the (slab fluid-metasomatized) lithospheric mantle, partial melting of the crust due to the intrusion of basaltic magmas, and widespread and voluminous volcanism (Bonin et al., 1998). Most of the silicic volcanism in the TPMP, and especially the Davis Mountains volcanic field, occurred between 39 and 36 Ma (Henry and McDowell, 1986; Henry et al., 1994). In the southern Rio Grande rift, New Mexico, this phase is represented by the eruption of the arc-like Rubio Peak Formation (McMillan et al., 2000).

(3) Post-orogenic (early "Asthenospheric Magmatism" phase of Lawton and McMillan, 1999). This phase, which represents the early stage of continental rifting, is characterized by uplift and an increase in bimodal and peralkaline volcanism, and is the result of delamination of the lithosphere and sinking of the detached lithosphere from 36–34 to ~27 Ma. The stress field shifted from weakly compressional or neutral to extensional and magma sources shifted from more lithospheric to more asthenospheric. The lack of development of normal fault-bounded sedimentary basins during early continental rifting could be due to decoupled behavior between the upper crust and the lower crust and upper mantle: Wilson et al. (2005) have shown that in the Rio Grande rift, extension in the lower crust is distributed over a region four times as wide as the crustal expression of extension. Thus, in the early stage of continental rifting, continental extension may have triggered magmatism in the upper mantle/lower crust long before that extension was manifested at the surface.

During the post-orogenic phase, the majority of volcanism in the TPMP is concentrated in the Big Bend area in both alkali-calcic (e.g., the 32 Ma Chinati Mountains caldera) and alkalic volcanic centers (Pine Canyon caldera) (Henry and McDowell, 1986). In the southern Rio Grande rift, this phase is represented by eruption of the bimodal basalt–rhyolite Bell Top Formation (McMillan et al., 2000). In the northern Rio Grande rift (San Juan Mountains, Colorado), lavas and tuffs of the Conejos Formation erupted between 35–33 Ma;

this high-K basalt–andesite–rhyolite suite evolved via fractional crystallization, assimilation, and partial melting processes (Parker et al., 2005). Silicic volcanism ended between 28.5 and 27 Ma in both southern New Mexico (McMillan et al., 2000) and in the TPMP (Leyva Canyon volcano: White and Urbanczyk, 2001), which also marked the end of the post-orogenic phase.

(4) Relaxation. In the final phase, a clearly extensional, intraplate regime characterized by normal faulting was established, and magma geochemistries reflected a greater influence from the asthenosphere and a smaller influence from the crust. Magmatism in the TPMP from 27 to 16 Ma was primarily mafic, more sporadic, and after 24 Ma was coeval with normal faulting (Henry and McDowell, 1986).

7. Summary

Two different petrogenetic mechanisms for generating peralkaline rocks operating nearly simultaneously have been identified as responsible for the origin of the South Rim Formation at the Pine Canyon caldera in Trans-Pecos Texas. Ultimately, both mechanisms begin with the intrusion of mantle-derived alkali basaltic magmas into the crust. Heat from the intrusion of basalt, coupled with metasomatism from a F-rich volatile phase, resulted in partial melting of deep (<25 km) crust mafic granulite. Approximately 5% partial melting of mafic granulite produced peralkaline high-silica rhyolite (Emory Peak Rhyolite Member), which differentiated via fractional crystallization of alkali feldspar, quartz, biotite, magnetite, zircon, and monazite. Alkali basalt evolved via ~70% fractional crystallization coupled with assimilation ($M_a/M_c \approx 0.4$) of shale wall-rock to produce peralkaline quartz trachyte (Boot Rock Member). Closed-system fractional crystallization (~70–75%) of the Boot Rock Member quartz trachyte at low fO_2 produced the more strongly peralkaline (A.I. = 1.21) rhyolite (Pine Canyon Rhyolite Member). The eruption of ash-flow tuffs of the Pine Canyon Rhyolite Member produced the Pine Canyon caldera (Ogley, 1978; Barker et al., 1986). Lavas and tuffs of the Boot Rock Member erupted shortly thereafter from vents both along the margin of the caldera and outside of the caldera (Urbanczyk and White, 2000). The final eruptive event is represented by rheomorphic ash-flow tuffs of the Emory Peak Rhyolite Member from vents both along the margin of the caldera and from an extensive ring dike outside of the caldera (Barker et al., 1986). The geochemical characteristics and petrogenetic mechanisms responsible for the development of the peralkaline magmas of the South Rim Formation are most consistent with those operating in continental rift environments. On the basis of these results coupled with petrologic, structural, and geophysical results from other workers in the region, these peralkaline rocks are interpreted to represent the earliest evidence for continental extension in the TPMP.

Acknowledgements

The authors thank Dan Barker, Nancy McMillan, and Gregor Markl for their very helpful comments and suggestions. We would also like to thank the organizers of and participants at PERALK, the international workshop on peralkaline magmatism sponsored by the Institut für Geowissenschaften, Universität Tübingen, Germany, held from March 4 to 6, 2005. The talks presented and discussions at the workshop proved to be a great and positive influence on the development on this paper. Funding for rock analyses and thin-sections was supported by a grant from the University Research Committee at Eastern Kentucky University. Funding for electron probe microanalyses was provided by NSF grant EAR-0116660 to the Department of Geological Sciences at the University of Texas at El Paso.

Appendix A. Supplementary data

Supplementary data associated with this article can be found, in the online version, at doi:10.1016/j.lithos.2006.03.015.

References

Adams, D.T., 2004. Field relations and geochemistry of peralkalic rhyolitic lava domes and flows and associated mafic lava in the southwestern portion of the Cerro Castellan 7 1/2 minute quadrangle: Big Bend National Park, west Texas. Unpublished M.S. thesis, Baylor University, Waco, Texas.

Allègre, C.J., Treuil, M., Minster, J.-F., Minster, B., Albarède, F., 1977. Systematic use of trace elements in igneous processes: Part I. fractional crystallization processes in volcanic suites. Contributions to Mineralogy and Petrology 60, 57–75.

Andersen, D.J., Lindsley, D.H., 1988. Internally consistent solution models for Fe–Mg–Mn–Ti oxides: Fe–Ti oxides. American Mineralogist 73, 714–726.

Andersen, D.J., Lindsley, D.H., Davidson, P.M., 1993. QUILF: a PASCAL program to assess equilibria among Fe–Mg–Mn–Ti oxides, pyroxenes, olivine, and quartz. Computers and Geosciences 19, 1333–1350.

Bailey, D.K., 1974. Melting in the deep crust. In: Sørensen, H. (Ed.), The Alkaline Rocks. John Wiley and Sons, New York, pp. 436–442.

Bailey, D.K., Macdonald, R., 1970. Petrochemical variations among mildly peralkaline (comendite) obsidians from the oceans and continents. Contributions to Mineralogy and Petrology 28, 340–351.

Bailey, D.K., Macdonald, R., 1975. Fluorine and chlorine in peralkaline liquids and the need for magma generation in an open system. Mineralogical Magazine 40, 405–414.

Bailey, D.K., Macdonald, R., 1987. Dry peralkaline felsic liquids and carbon dioxide flux through the Kenya Rift Zone. In: Mysen, B.O. (Ed.), Magmatic Processes: Physiochemical Principles. Geochemical Society Special Publication, vol. 1, pp. 91–105.

Barker, D.S., 1977. Northern Trans-Pecos Magmatic Province: introduction and comparison with the Kenya Rift. Geological Society of America Bulletin 88, 1421–1427.

Barker, D.S., 1987. Tertiary alkaline magmatism in Trans-Pecos Texas. In: Fitton, J.G., Upton, B.G.J. (Eds.), Alkaline Igneous Rocks. Special Publication, vol. 30. Geological Society, London, pp. 415–431.

Barker, D.S., 2000. Down to Earth at Tuff Canyon, Big Bend National Park, Texas. University of Texas at Austin Bureau of Economic Geology, DE 2. 40 pp.

Baker, B.H., Goles, G.G., Leeman, W.P., Lindstrom, M.M., 1977. Geochemistry and petrogenesis of a basalt–benmoreite–trachyte suite from the southern part of the Gregory Rift, Kenya. Contributions to Mineralogy and Petrology 64, 303–332.

Barker, D.S., Henry, C.D., McDowell, F.W., 1986. Pine Canyon caldera, Big Bend National Park: a mildly peralkaline magmatic system. In: Price, J.G., Henry, C.D., Parker, D.F., Barker, D.S. (Eds.), Igneous Geology of Trans-Pecos Texas: Field Trip Guide and Research Articles. University of Texas at Austin Bureau of Economic Geology Guidebook, vol. 23, pp. 266–285.

Bea, F., Pereira, M.D., Stroh, A., 1994. Mineral/leucosome trace-element partitioning in a peraluminous migmatite (a laser ablation-ICP-MS study). Chemical Geology 117, 291–312.

Benker, S.C., 2005. The petrology of the South Rim Formation, Big Bend National Park, Texas. Unpublished M.S. Thesis, Eastern Kentucky University, Richmond.

Bohrson, W.A., Reid, M.R., 1997. Genesis of silicic peralkaline volcanic rocks in an ocean island setting by crustal melting and open-system processes: Socorro Island, Mexico. Journal of Petrology 38, 1137–1166.

Bohrson, W.A., Reid, M.R., 1998. Genesis of evolved ocean island magma by deep- and shallow-level basement recycling, Socorro Island, Mexico: constraints from Th and other isotope signatures. Journal of Petrology 39, 995–1008.

Bonin, B., 1988. From orogenic to anorogenic environments: evidence from associated magmatic episodes. Schweizerische Mineralogische und Petrographische Mitteilungen 68, 301–311.

Bonin, B., 2004. Do coeval mafic and felsic magmas in post-collisional to within-plate regimes necessarily imply two contrasting, mantle and crustal, sources? A review. Lithos 78, 1–24.

Bonin, B., Azzouni-Sekkal, A., Bussy, F., Ferrag, S., 1998. Alkali-calcic and alkaline post-orogenic (PO) granite magmatism: petrologic constrains and geodynamic settings. Lithos 45, 45–70.

Bowden, P., 1974. Oversaturated alkaline rocks: granites, pantellerites, and comendites. In: Sørensen, H. (Ed.), The Alkaline Rocks. John Wiley and Sons, New York, pp. 109–123.

Boynton, W.V., 1984. Geochemistry of the rare earth elements: meteorite studies. In: Henderson, P. (Ed.), Rare Earth Element Geochemistry. Elsevier, pp. 63–114.

Bradshaw, T.K., 1992. The adaptation of Pearce element ratio diagrams to complex high silica systems. Contributions to Mineralogy and Petrology 109, 450–458.

Bryan, W.B., Finger, L.W., Chayes, F., 1969. Estimating proportions in petrographic mixing equations by least-squares approximation. Science 163, 926–927.

Cadoux, A., Pinti, D.L., Aznar, C., Chiesa, S., Gillot, P.-Y., 2005. New geochronological and geochemical constraints on the genesis and geological evolution of Ponza and Palmarola volcanic islands (Tyrrhenian Sea, Italy). Lithos 81, 121–151.

Cameron, K.L., Robinson, J.V., Niemeyer, S., Nimz, G.J., Kuentz, D.C., Harmon, R.S., Bohlen, S.R., Collerson, K.D., 1992. Contrasting styles of pre-Cenozoic and mid-Tertiary crustal evolution in northern Mexico: evidence from deep crustal xenoliths from La Olivina. Journal of Geophysical Research 97, 17353–17376.

Chapin, C.E., Wilks, M., McIntosh, W.C., 2004. Space-time patterns of Late Cretaceous to present magmatism in New Mexico — comparison with Andean volcanism and potential for future volcanism. New Mexico Bureau of Geology and Mineral Resources, Bulletin 160, 13–40.

Charles, R.W., 1975. The phase equilibria of richterite and ferrorichterite. American Mineralogist 60, 367–374.

Civetta, L., D'Antonio, M., Orsi, G., Tilton, G.R., 1998. The geochemistry of volcanic rocks from Pantelleria Island, Sicily Channel: petrogenesis and characteristics of the mantle source region. Journal of Petrology 39, 1453–1491.

Condie, K.C., 1993. Chemical composition and evolution of the upper continental crust: contrasting results from surface samples and shales. Chemical Geology 104, 1–37.

Coney, P.J., Reynolds, S.J., 1977. Cordilleran Benioff zones. Nature 270, 403–406.

Dachs, E., 1994. Annite stability revised: 1. Hydrogen-sensor data for the reaction annite=sanidine+magnetite+H_2. Contributions to Mineralogy and Petrology 117, 229–240.

Davies, G.R., Macdonald, R., 1987. Crustal influences in the petrogenesis of the Naivasha basalt–comendite complex: combined trace element and Sr–Nd–Pb isotope constraints. Journal of Petrology 28, 1009–1031.

Deer, W.A., Howie, R.A., Zussman, J., 1966. An Introduction to the Rock-Forming Minerals. John Wiley and Sons, Inc., New York, NY.

DePaolo, D.J., 1981. Trace element and isotopic effects of combined wallrock assimilation and fractional crystallization. Earth and Planetary Science Letters 53, 189–202.

Dickerson, P.W., Muehlberger, W.R., 1994. Basins in the Big Bend segment of the Rio Grande rift, Trans-Pecos Texas. In: Keller, G. R., Cather, S.M. (Eds.), Basins of the Rio Grande Rift: Structure, Stratigraphy, and Tectonic Setting. Geological Society of America Special Paper, vol. 291, pp. 283–297.

Drenth, B.J., Finn, C.A., 2004. Interpretation of aeromagnetic anomalies over the Pine Canyon caldera, Big Bend National Park, Texas. Geological Society of America Abstracts with Programs 36 (5), 127.

Dungan, M.A., Lindstrom, M.M., McMillan, N.J., Moorbath, S., Hoefs, J., Haskin, L.A., 1986. Open system magmatic evolution of the Taos Plateau Volcanic Field, northern New Mexico: 1. The petrology and geochemistry of the Servilleta Basalt. Journal of Geophysical Research 91, 5999–6028.

Ebinger, C.J., Yemane, T., Harding, D.J., Tesfaye, S., Kelley, S., Rex, D.C., 2000. Rift deflection, migration, and propagation: linkage of the Ethiopian and Eastern rifts, Africa. Geological Society of America Bulletin 112, 163–176.

Eichelberger, J.C., 1978. Andesitic volcanism and crustal evolution. Nature 275, 21–27.

Evans, O.C., Hanson, G.N., 1993. Accessory-mineral fractionation of rare-earth element (REE) abundances in granitoid rocks. Chemical Geology 110, 69–93.

Fujimaki, H., 1986. Partition coefficients of Hf, Zr, and REE between zircon, apatite, and liquid. Contributions to Mineralogy and Petrology 94, 42–45.

Greenland, L.P., 1970. An equation for trace element distribution during magmatic crystallization. American Mineralogist 55, 455–465.

Hay, D.E., Wendlandt, R.F., 1995. The origin of Kenya rift plateau-type flood phonolites: results of high-pressure/high-temperature experiments in the systems phonolite–H_2O and phonolite–H_2O–CO_2. Journal of Geophysical Research 100, 401–410.

Hay, D.E., Wendlandt, R.F., Keller, G.R., 1995a. Origin of Kenya rift plateau-type flood phonolites: integrated petrologic and geophysical constraints on the evolution of the crust and upper mantle beneath the Kenya rift. Journal of Geophysical Research 100, 10,549–10,557.

Hay, D.E., Wendlandt, R.F., Wendlant, E.D., 1995b. The origin of Kenya rift plateau-type flood phonolites: evidence from geochemical studies for fusion of lower crust modified by alkali basaltic magmatism. Journal of Geophysical Research 100, 411–422.

Henry, C.D., Davis, L.L., 1996. Tertiary volcanic, volcaniclastic, and intrusive rocks adjacent to the Solitario. In: Henry, C.D., Muehlberger, W.R. (Eds.), Geology of the Solitario Dome, Trans-Pecos Texas: Paleozoic, Mesozoic, and Cenozoic Sedimentation, Tectonism, and Magmatism. University of Texas at Austin Bureau of Economic Geology Report of Investigations, vol. 240, pp. 81–105.

Henry, C.D., McDowell, F.W., 1986. Geochronology of magmatism in the Tertiary volcanic field, Trans-Pecos Texas. In: Price, J.G., Henry, C.D., Parker, D.F., Barker, D.S. (Eds.), Igneous Geology of Trans-Pecos Texas: Field Trip Guide and Research Articles. University of Texas at Austin Bureau of Economic Geology Guidebook, vol. 23, pp. 99–122.

Henry, C.D., Price, J.G., 1986. Early Basin and Range development in Trans-Pecos Texas and adjacent Chihuahua: magmatism and orientation, timing, and style of extension. Journal of Geophysical Research 91, 6213–6224.

Henry, C.D., Price, J.G., Parker, D.F., Wolff, J.A., 1989. Mid-Tertiary silicic alkalic magmatism of Trans-Pecos Texas: rheomorphic tuffs and extensive silicic lavas. In: Chapin, C.E., Zidek, J. (Eds.), Field Excursions to Volcanic Terranes in the Western United States. Volume I: Southern Rocky Mountain Region. New Mexico Bureau of Mines and Mineral Resources Memoir, vol. 46, pp. 231–274.

Henry, C.D., Price, J.G., James, E.W., 1991. Mid-Cenozoic stress evolution and magmatism in the southern Cordillera, Texas and Mexico: transition from continental arc to intraplate extension. Journal of Geophysical Research 96, 13,545–13,560.

Henry, C.D., Kunk, M.J., McIntosh, W.C., 1994. $^{40}Ar/^{39}Ar$ chronology and volcanology of silicic volcanism in the Davis Mountains, Trans-Pecos Texas. Geological Society of America Bulletin 106, 1359–1376.

Hildreth, W., 1981. Gradients in silicic magma chambers: implications for lithospheric magmatism. Journal of Geophysical Research 86, 10,153–10,192.

Holt, G.S., 1998. Trace element partitioning of alkali feldspar in Burro Mesa Rhyolite and other units of the Trans-Pecos Magmatic Province. Unpublished M.S. Thesis, Baylor University, Waco, Texas.

Houghton, B.F., Weaver, S.D., Wilson, C.J.N., Lanphere, M.A., 1992. Evolution of a Quaternary peralkaline volcano: Mayor Island, New Zealand. Journal of Volcanology and Geothermal Research 51, 217–236.

James, E.W., Henry, C.D., 1991. Compositional changes in Trans-Pecos Texas magmatism coincident with Cenozoic stress realignment. Journal of Geophysical Research 96, 13,561–13,575.

James, E.W., Henry, C.D., 1993. Southeastern extent of the North American craton in Texas and northern Chihuahua as revealed by Pb isotopes. Geological Society of America Bulletin 105, 116–126.

Lawton, T.F., McMillan, N.J., 1999. Arc abandonment as a cause for passive rifting: comparison of the Jurassic Mexican borderland rift and the Cenozoic Rio Grande rift. Geology 27, 779–782.

Le Maitre, R.W., Streckeisen, A., Zanettin, B., Le Bas, M.J., Bonin, B., Bateman, P., Bellieni, G., Dudek, A., Efremova, S., Keller, J., Lameyre, J., Sabine, P.A., Schmid, R., Sørensen, H., Woolley, A.R., 2002. Igneous Rocks: A Classification and Glossary of Terms: Recommendations of the International Union of Geological Sciences Subcommission on the Systematics of Igneous Rocks. Cambridge University Press. 236 pp.

Loiselle, M.C., Wones, D.R., 1979. Characteristics and origin of anorogenic granites. Geological Society of America Abstracts with Programs 11 (7), 468.

Lowenstern, J.B., Mahood, G.A., 1991. New data on magmatic H_2O contents of pantellerite, with implications for petrogenesis and eruptive dynamics at Pantelleria. Bulletin of Volcanology 54, 78–83.

Lueth, V.W., Rye, R.O., Peters, L., 2005. "Sour gas" hydrothermal jarosite: ancient to modern acid-sulfate mineralization in the southern Rio Grande Rift. Chemical Geology 215, 339–360.

Macdonald, R., Davies, G.R., Bliss, C.M., Leat, P.T., Bailey, D.K., Smith, R.L., 1987. Geochemistry of high-silica peralkaline rhyolites, Naivasha, Kenya Rift Valley. Journal of Petrology 28, 979–1008.

Mahood, G.A., Stimac, J.A., 1990. Trace-element partitioning in pantellerites and trachytes. Geochimica et Cosmochimica Acta 54, 2257–2276.

Martin, R.F., 2006. A-type granites are ultimately results of open-system fenitization-type reactions in a rift environment. Lithos 91, 125–136. (this volume) doi:10.1016/j.lithos.2006.03.012.

Maxwell, R.A., Lonsdale, J.T., Hazzard, R.T., Wilson, J.A., 1967. Geology of Big Bend National Park, Texas. University of Texas at Austin Bureau of Economic Geology Publication, vol. 6711. 320 pp.

McIntosh, W.C., Chapin, C.E., 2004. Geochronology of the central Colorado volcanic field. New Mexico Bureau of Geology and Mineral Resources, Bulletin 160, 2058–2237.

McKenzie, D., O'Nions, R.K., 1991. Partial melt distributions from inversion of rare earth element concentrations. Journal of Petrology 32, 1021–1091.

McMillan, N.J., Dickin, A.P., Haag, D., 2000. Evolution of magma source regions in the Rio Grande rift, southern New Mexico. Geological Society of America Bulletin 112, 1582–1593.

Miggins, D., Scott, R.B., Snee, L.W., 2004. New $^{40}Ar/^{39}Ar$ ages from Big Bend National Park. Geological Society of America Abstracts with Programs 36 (5), 128.

Minster, J.-F., Allègre, C.J., 1978. Systematic use of trace elements in igneous processes: Part III. Inverse problem of batch partial melting in volcanic suites. Contributions to Mineralogy and Petrology 68, 37–52.

Mungall, J.E., Martin, R.F., 1995. Petrogenesis of basalt–comendite and basalt–pantellerite series, Terceira Azores, and some implications for the origin of ocean–island rhyolites. Contributions to Mineralogy and Petrology 119, 43–55.

Nelson, D.O., Nelson, K.L., Reeves, K.D., Mattison, G.D., 1987. Geochemistry of Tertiary alkaline rocks of the eastern Trans-Pecos magmatic province, Texas. Contributions to Mineralogy and Petrology 97, 72–97.

Ogley, D.S., 1978. Eruptive history of the Pine Canyon caldera, Big Bend National Park, Texas. Unpublished M.A. Thesis, University of Texas at Austin.

Parker, D.F., 1983. The origin of the trachyte–quartz trachyte–peralkaline rhyolite suite of the Oligocene Paisano volcano, Trans-Pecos Texas. Geological Society of America Bulletin 94, 614–629.

Parker, D.F, 1986. Stratigraphic, structural, and petrologic development of the Buckhorn caldera, northern Davis Mountains, Trans-Pecos Texas. In: Price, J.G., Henry, C.D., Parker, D.F., Barker, D.S. (Eds.), Igneous Geology of Trans-Pecos Texas, the University of Texas at Austin Bureau of Economic Geology Guidebook, vol. 23, pp. 286–302.

Parker, D.F., 2002. Horseshoe Canyon volcanic dome. In: White, J.C. (Ed.), The Geology of Big Bend National Park: What Have We Learned Since Maxwell and Others (1967)? Field Trip Guide, Geological Society of America South-Central Meeting, Alpine, Texas, pp. 24–32.

Parker, D.F., Ghosh, A., Price, C.W., Rinard, B.D., Cullers, R.L., Ren, M., 2005. Origin of rhyolite by crustal melting and the nature of parental magmas in the Oligocene Conejos Formation, San Juan Mountains, Colorado, USA. Journal of Volcanology and Geothermal Research 139, 185–210.

Paster, T.P., Schauwecker, D.S., Haskin, L.A., 1974. The behavior of some trace elements during solidification of the Skaergaard layered series. Geochimica et Cosmochimica Acta 38, 1549–1577.

Pearce, T.H., 1968. A contribution to the theory of variation diagrams. Contributions to Mineralogy and Petrology 19, 142–157.

Pearce, J.A., Norry, M.J., 1979. Petrogenetic implications of Ti, Zr, Y, and Nb variations in volcanic rocks. Contributions to Mineralogy and Petrology 69, 33–47.

Pearce, J.A., Harris, N.B.W., Tindle, A.G., 1984. Trace element discrimination diagrams for the tectonic interpretation of granitic rocks. Journal of Petrology 25, 956–983.

Peccerillo, A., Barberio, M.R., Yirgu, G., Ayalew, D., Barbieri, M., Wu, T.W., 2003. Relationships between mafic and peralkaline silicic magmatism in continental rift settings: a petrological, geochemical, and isotopic study of the Gedemsa Volcano, central Ethiopian Rift. Journal of Petrology 44, 2003–2032.

Potter, L.S., 1996. Chemical variation along strike in feldspathoidal rocks of the eastern alkalic belt, Trans-Pecos Magmatic Province, Texas and New Mexico. The Canadian Mineralogist 34, 241–264.

Russell, J.K., Nicholls, J., 1988. Analysis of petrologic hypotheses with Pearce element ratios. Contributions to Mineralogy and Petrology 99, 25–35.

Scaillet, B., Macdonald, R., 2001. Phase relations of peralkaline silicic magmas and petrogenetic implications. Journal of Petrology 42, 825–845.

Scaillet, B., Macdonald, R., 2003. Experimental constraints on the relationships between peralkaline rhyolites of the Kenya Rift Valley. Journal of Petrology 44, 1867–1894.

Schucker, D.E., 1986. Geochemistry and petrogenesis of the mafic flow units within the Chisos Formation, Big Bend National Park, Texas. Unpublished M.S. thesis, Sul Ross State University, Alpine, Texas.

Schucker, D.E., Nelson, D.O., 1988. New potassium–argon dates of mafic rocks within Big Bend National Park, Texas. Texas Journal of Science 40, 71–78.

Schnetzler, C.C., Philpotts, J.A., 1970. Partition coefficients of rare-earth elements between igneous matrix material and rock-forming mineral phenocrysts: II. Geochimica et Cosmochimica Acta 34, 331–340.

Smith, I.E.M., Chappell, B.W., Ward, G.K., Freeman, R.S., 1977. Peralkaline rhyolites associated with andesitic arcs of the southwest Pacific. Earth and Planetary Science Letters 37, 230–236.

Sobolev, A.V., Migdisov, A.A., Portnyagin, M.V., 1996. Incompatible element partitioning between clinopyroxene and basalt liquid revealed by the study of melt inclusions in minerals from Troodos lavas, Cyprus. Petrology 4, 307–317.

Stanley, C.R., Russell, J.K., 1990. Matrix methods for the development of Pearce element ratio diagrams. In: Stanley, C.R., Russell, J.K. (Eds.), Theory and Application of Pearce Element Ratios to Geochemical Data Analysis. Geological Association of Canada Short Course, vol. 8, pp. 131–156.

Stolz, A.J., Davies, G.R., Crawford, A.J., Smith, I.E.M., 1993. Sr, Nd and Pb isotopic compositions of calc-alkaline and peralkaine silicic volcanics from the D'Entrecasteaux Islands, Papua New Guinea, and their tectonic significance. Mineralogy and Petrology 47, 103–126.

Thompson, R.N., 1982. Magmatism of the British Tertiary volcanic province. Scottish Journal of Geology 18, 49–107.

Urbanczyk, K.M., White, J.C., 2000. Pine Canyon caldera, Big Bend National Park, Texas: a new interpretation. Geological Society of America Abstracts with Programs 32 (3), 43.

Villemant, B., 1988. Trace-element evolution in the Phlegrean Fields (central-Italy) — fractional crystallization and selective enrichment. Contributions to Mineralogy and Petrology 98, 169–183.

Villemant, B., Jaffrezic, H., Joron, J.L., Treuil, M., 1981. Distribution coefficients of major and trace-elements — fractional crystallization in the alkali basalt series of Chaine-Des-Puys (Massif Central, France). Geochimica et Cosmochimica Acta 45, 1997–2016.

Walker, G.P.L., 1984. Downsag calderas, ring faults, caldera sizes, and incremental caldera growth. Journal of Geophysical Research 89, 8407–8416.

Ward, P.L., 1991. On plate tectonics and the geologic evolution of southwestern North America. Journal of Geophysical Research 96, 12,479–12,496.

Wark, D.A., Miller, C.F., 1993. Accessory mineral behavior during differentiation of a granite suite: monazite, xenotime, and zircon in the Sweetwater Wash pluton, southeastern California, U.S.A. Chemical Geology 110, 49–67.

Whalen, J.B., Currie, K.L., Chappell, B.W., 1987. A-type granites: geochemical characteristics, discrimination, and petrogenesis. Contributions to Mineralogy and Petrology 95, 407–419.

White, J.C., 2003. Trace-element partitioning between alkali feldspar and peralkalic quartz trachyte to rhyolite magma: Part II. Empirical equations for calculating trace-element partition coefficients of large-ion lithophile, high field-strength, and rare-earth elements. American Mineralogist 88, 330–337.

White, J.C., Urbanczyk, K.M., 2001. Origin of a silica-oversaturated quartz trachyte–rhyolite suite through combined crustal melting, magma mixing, and fractional crystallization: the Leyva Canyon volcano, Trans-Pecos Magmatic Province, Texas. Journal of Volcanology and Geothermal Research 111, 155–182.

White, J.C., Holt, G.S., Parker, D.F., Ren, M., 2003. Trace-element partitioning between alkali feldspar and peralkalic quartz trachyte to rhyolite magma: Part I. Systematics of trace-element partitioning. American Mineralogist 88, 316–329.

White, J.C., Ren, M., Parker, D.F., 2005. Variation in mineralogy, temperature, and oxygen fugacity in a suite of strongly peralkaline lavas and tuffs, Pantelleria, Italy. The Canadian Mineralogist 43, 1331–1347.

Wilson, D., Aster, R., West, M., Ni, J., Grand, S., Gao, W., Baldridge, W.S., Semken, S., Patel, P., 2005. Lithosphere structure of the Rio Grande rift. Nature 433, 851–855.